Journal of Constructional Steel Research 213 (2024) 108375

Contents lists available at ScienceDirect

Journal of Constructional Steel Research

journal homepage: www.elsevier.com/locate/jcsr

Design optimisation for cold rolled steel beam sections with web and flange stiffeners

S.J. Qadir [a,c], V.B. Nguyen [a,*], I. Hajirasouliha [b]

[a] College of Science and Engineering, University of Derby, Markeaton Street, Derby DE22 3AW, United Kingdom
[b] Department of Civil and Structural Engineering, The University of Sheffield, Sir Frederick Mappin Building, Mappin Street, Sheffield S1 3JD, United Kingdom
[c] Civil Engineering Department, College of Engineering, University of Sulaimani, Iraq

ARTICLE INFO

Keywords:
Cold working effect
Material testing
Cold rolled section
Complex stiffeners
Flexural strength
Finite element modelling
Optimisation

ABSTRACT

This paper presents the analysis and design optimisation of the cold rolled steel sections for flexural strength considering the effect of cold working exerted on the section during the roll forming process. The sections included channel and zed shapes with complex longitudinal web and flange stiffeners. Nonlinear Finite Element (FE) modelling was developed to model the flexural strength of the channel and zed beams and validated against the four-point bending experiments for these sections. The material properties of steel at the section's flat parts, corners, and stiffener bends were obtained from tensile tests and were incorporated into the FE simulations to account for the true material properties at these regions due to the cold working during the roll forming process. The strength enhancement at the section corners and stiffener bends obtained from tensile tests were also compared with the predicted values from design standards. The section strength was then optimised using FE modelling results based on the Design Of Experiments (DOE) and response surface methodology. Optimal designs for the channel and zed sections with maximum strength in distortional buckling could be obtained while changing the stiffeners' position, shape, sizes, and considering true material properties at section corners and stiffener bends. It revealed that, for the two sets of channel and zed sections with the depths of 145 mm and 170 mm, the optimal designs provided up to 43% and 39% increase in flexural strength for the channel and zed sections, respectively; however, when the true material properties at the section corner and the stiffener's bend regions was included, the increase in flexural strength increased up to 50% and 41%, respectively. Including flange stiffeners to the sections with longitudinal web stiffeners generally increased further the section strength. However, the levels of increase were largely dependent on the section depths and material properties.

1. Introduction

Cold rolled beam sections, i.e. purlins in building frame systems, are usually manufactured by the cold roll forming process into conventional channel and zed profiles. The flat elements of these sections have large width-to-thickness ratios, so they are prone to local or distortional buckling that govern the failure modes. A main method to improve the strength of cold rolled sections is including longitudinal stiffeners at the web and/or flange of the sections. These stiffeners subdivide the flat elements of the web and flange so it can significantly increase the local buckling load of sections under compressive stresses (due to the smaller width-to-thickness ratio of the sub-elements). Sections could have "standard" stiffeners such as symmetrical angle, i.e. pre-qualified profiles as defined in codes of practice [1–3] or "complex" stiffeners such as unsymmetrical angles with many curved bends or semi-circular shapes [4]. There have been extensive investigations on buckling and ultimate strengths and design of sections with web stiffeners; however, most of them are for columns under compression and there have been limited investigations on channel and zed sections with stiffeners subjected to bending [5–8].

Only a few studies considered intermediate stiffeners in the flanges of channel and zed beams [9]. Practical design methods for these sections including the Effective Width Method or the Direct Strength Method, are normally specified in codes of practice in different countries such as European Standard [1], North American Specification and Australian/New Zealand Standard [3]. However, the Direct Strength Method is more applicable for sections that contain complex stiffeners as using the Effective Width Method for these sections is very complicated and

* Corresponding author.
E-mail address: vb.nguyen@derby.ac.uk (V.B. Nguyen).

https://doi.org/10.1016/j.jcsr.2023.108375
Received 17 September 2023; Received in revised form 16 November 2023; Accepted 23 November 2023
Available online 12 December 2023

impractical in calculating the effective section properties [10]. The Finite Element (FE) method has been widely used in analysis and design of cold formed steel structures, however, there have been limited studies for cold-formed steel sections with stiffeners in bending. The study [11] applied the FE analysis through ABAQUS software to provide further understanding on the behaviour of intermediately stiffened elements of hat sections under pure bending. The study [9] carried out a series of nonlinear FE analyses to investigate the flexural behaviour of cold-formed Z sections with intermediate stiffeners in their flanges. Recent investigations on buckling and ultimate strengths for channel and zed sections with stiffeners using Finite Element analysis were presented in [12,13].

During the cold rolled forming process, different levels of cold working or plastic deformation in material are generated, resulting in changes to the mechanical properties of the virgin coil material. Significant amounts of plastic deformation are found in the regions around section corners and stiffener bends in comparison to the flat counterpart regions, hence resulting in an increase in material yield and ultimate strengths, but a decrease in material ductility. Over the last few decades, there have been many studies conducted to quantify the cold working effect in the curved regions of metallic material and develop several models to predict the strength enhancement. The most widely used of which are for the stainless-steel sections [14–24] and the carbon-steel sections [25–36]. Several studies have investigated the cold formed sections, where the cold working effect on mechanical properties of the material and their effects on structural behaviour of the sections were quantified. Some studies measured the strength enhancement in the section corners and pointed out that it had negligible influences on load-bearing capacity of structural column members [28,34,35]. Other studies, have shown significant influences of cold working on load-bearing capacity of structural column members [14–16,18,21,22,24,27,29–32,37,38] and beam member [33].

In the cold roll forming industry, there is a critical requirement that is to reduce the initial strip to a minimum while maintaining/ increasing the structural performance of the roll formed products, thus minimising the major financial outlay in the process which is the material cost. Design optimisation of a cold rolled section can be achieved through a process of searching for alternative shapes to obtain its maximum strength while maintaining the same strip width (weight), leading to the most economical and efficient structure. Optimisation methods including Genetic Algorithms and Particle Swarm Optimisation were used together with the analytical methods available in design codes (the Effective Width Method or the Direct Strength Method) [1–3] to search for optimal designs with flexural strength target [6–8,39]. However, this approach was rather applicable for pre-defined profiles in which the dimensions of web, flanges, lips, and stiffeners were symmetrical and, in the dimension and shape ranges required by design standards. It is also noted that the current design methods [1–3] are limited in their ability to calculate the strength of channel and zed sections with symmetrical stiffeners.

In addition, most of previous studies on the optimisation of cold rolled sections did not consider both the geometry and the cold working influences on the section strengths, resulting in not very accurate optimisation results. Only the recently published studies [10,12,13] utilised FE modelling and optimisation techniques to determine the influences of the stiffener's geometry and cold working at the section corners and stiffener bends; the stiffener's geometry included its location, shape, and size. However, in these studies, the material properties of section corners and stiffener bends were not available from the tests. Therefore, the formulae from the North American specification [2] were used to calculate the material properties of corners and stiffener bends from those of the flat regions. While providing useful information on the effect of stiffener geometry and cold working, it did not provide accurate figures on the true material properties at section corners and stiffener bends, and subsequently, on the optimal design for flexural strength of these sections. In addition, there has not been work of analysis and optimisation for cold formed sections that included flange's intermediate stiffeners.

Therefore, the work in this study is driven by the need to develop the design optimisation for flexural strength of cold rolled steel beam sections with intermediate stiffeners considering the true material properties at section corners and stiffener bends generated during the roll forming process. The analysis and optimisation also focused upon the effects of including flange's stiffeners on the section strength. The design optimisation of two sets of industrial channel and zed beam sections having different depths, subjected to bending are presented to gain more generalised conclusions about the optimisation. Tensile tests of specimens extracted from the channel and zed beam sections' flat parts, corners, and stiffener bends were first carried out to obtain material properties at these regions. The increase in yield strength at the section corners and stiffener bends obtained from tensile tests were evaluated against the predicted value from design standards. Four-point bending tests for these sections were conducted to achieve the section flexural strengths.

Nonlinear FE models were then developed for channel and zed beams subjected to four-point bending tests and these models, the true material properties at section corners and stiffener bends, were validated against experimental test data. The verified FE models were then used for design optimisation which was carried out in three stages: (1) the sections were then parameterised in terms of geometric dimensions and material properties at section corners and stiffener bends, against the target responses which were the buckling and ultimate strengths of the sections, (2) the Design Of Experiments (DOE) and response surface were used to determine the influences of the section and stiffener's parameters on the section distortional buckling and flexural strength (in this approach, the dimensions, the initial imperfections, and the material properties at different parts of the sections were defined as input parameters while the buckling and flexural developed stresses were defined as output parameters), (3) a multi-objective genetic algorithm method was deployed to obtain optimal designs for the sections with maximum buckling and ultimate strengths while keeping the same amount of material used while changing the stiffeners' position, shape, sizes, and considering material properties at section corners and stiffener bends. Optimal cross-sectional shapes of the longitudinally stiffened channel and zed sections were finally selected and proposed.

2. Experimental test programme

The beam specimens were cold roll formed along the rolling direction on steel coils. The cross sections of the channel section and the zed section with generic dimensions, are shown in Fig. 1. For the channel section with a depth of 145 mm and a thickness of 1.2 mm, it was labelled as C-W145T1.2, and for the zed section with a depth of 145 mm and a thickness of 1.2 mm, it was labelled as Z-W145T1.2. The label C-W145T1.2 is described as follows: C: Channel specimen; W: Web, 145: Nominal web height or beam depth (mm); T: Thickness, 1.2: Nominal plate thickness (mm). Dim A is the distance from the peak of the stiffener to the upper hole of the web, Dim B is the distance between the web stiffeners, Dim C is the distance between the holes of the web, and Dim D is the length of the web. The specific dimensions of cross sections of the tested channel and zed specimens are shown in Figs. 6(a),(b), and Figs. 7 (a),(b), respectively.

2.1. Tensile tests

The material properties of flat parts, corners, and stiffener bends cut from the beam sections C-W145T1.2 and Z-W145T1.2 in the longitudinal direction of the finished sections, were obtained from tensile tests. For each type of beam section, the positions of the extracted specimens from the selected sections are shown in Fig. 2. The specimen identification system begins with the specimen type (web, flange, and corner), followed by the specimen locations in the longitudinal direction for

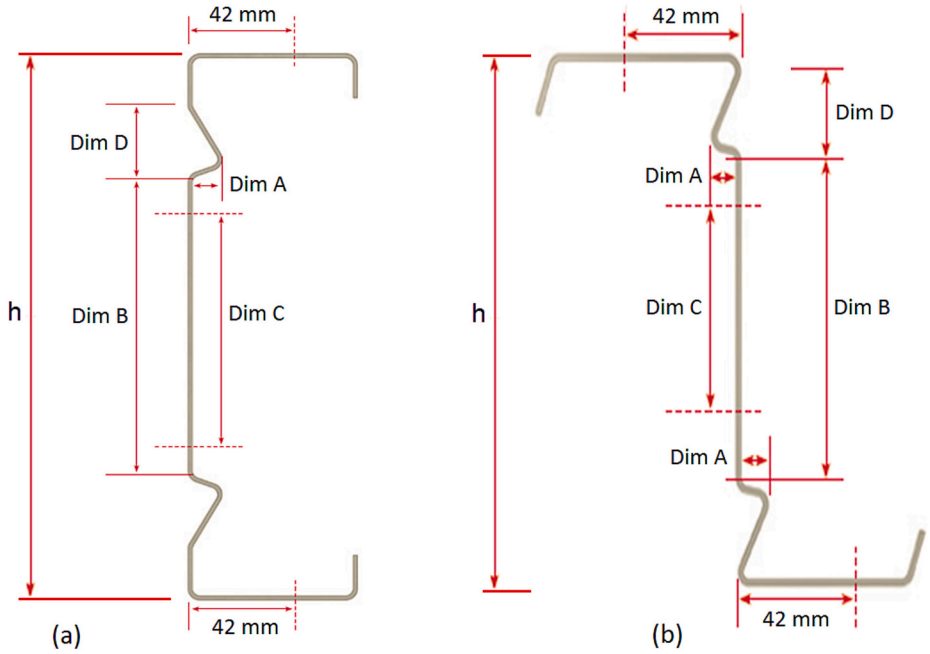

Fig. 1. Cross sections and geometries of beam specimens (a) 145 mm deep channel sections, and (b) 145 mm deep zed sections. 42 mm is the distance from the back of the section to the holes in the flange in the longitudinal direction.

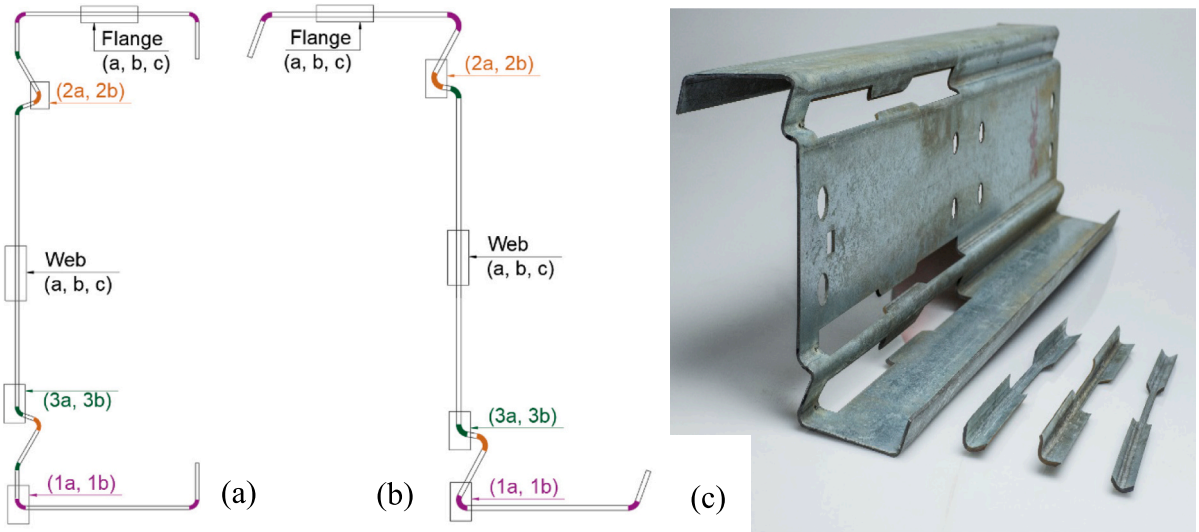

Fig. 2. Locations of extracted tensile specimens (a) channel cross section, (b) zed cross section, and (c) typical curved specimens wired cutting from the section Z-W145T1.2 and specimens extracted from curved locations 1, 2, and 3.

repeated tests, labelled as a, b, c. Three flat specimens were extracted from the centre line of the web; three flat specimens were extracted from the centre line of the flange; two corner specimens were taken from the section corners (web-flange junctions) at position 1; two curved specimens were taken from the most bent corner of the web stiffener at position 2; two curved specimens were taken from the second most bent corner of the web stiffener at position 3. Flat and curved steel specimens had the 'dog bone' shape and were prepared according to the appropriate specifications of the relevant European standard ISO 6892-1 (ISO 2009). The flat specimens had a parallel length of 75 mm and a width of 12.50 mm of the parallel length, while the curved specimens had a parallel length of 75 mm and a width of different dimensions depending on the positions and sizes of the cross sections, ranging from 3.5 to 12.5 mm.

A 50 mm gauge-length extensometer was attached to the tensile specimen. Each specimen was instrumented with linear 10-mm strain gauges on each side of the specimen at mid-length of the parallel part using TML strain gauge adhesive of CN series (Tokyo Measuring Instruments Laboratory Co., Ltd.) to measure the strains in the initial part of the stress-strain curve, as shown in Fig. 3. For cold roll-formed section members, the presence of residual stresses could result in different strains obtained from the two surfaces of the specimen. Therefore, strain gauges were attached onto both surfaces of each specimen and the average values of their readings were used to determine the strain values. For curved samples, due to the asymmetric shape of the curved specimens, they were tested in pairs (to avoid introducing unwanted bending moments) with a round bar with special knurled surfaces placed between the gripped ends of the specimens, as illustrated in Fig. 3.

The tensile specimens were tested in a 300-kN universal testing machine (Shimadzu AGS-X, Kyoto, Japan), with a displacement rate of 1

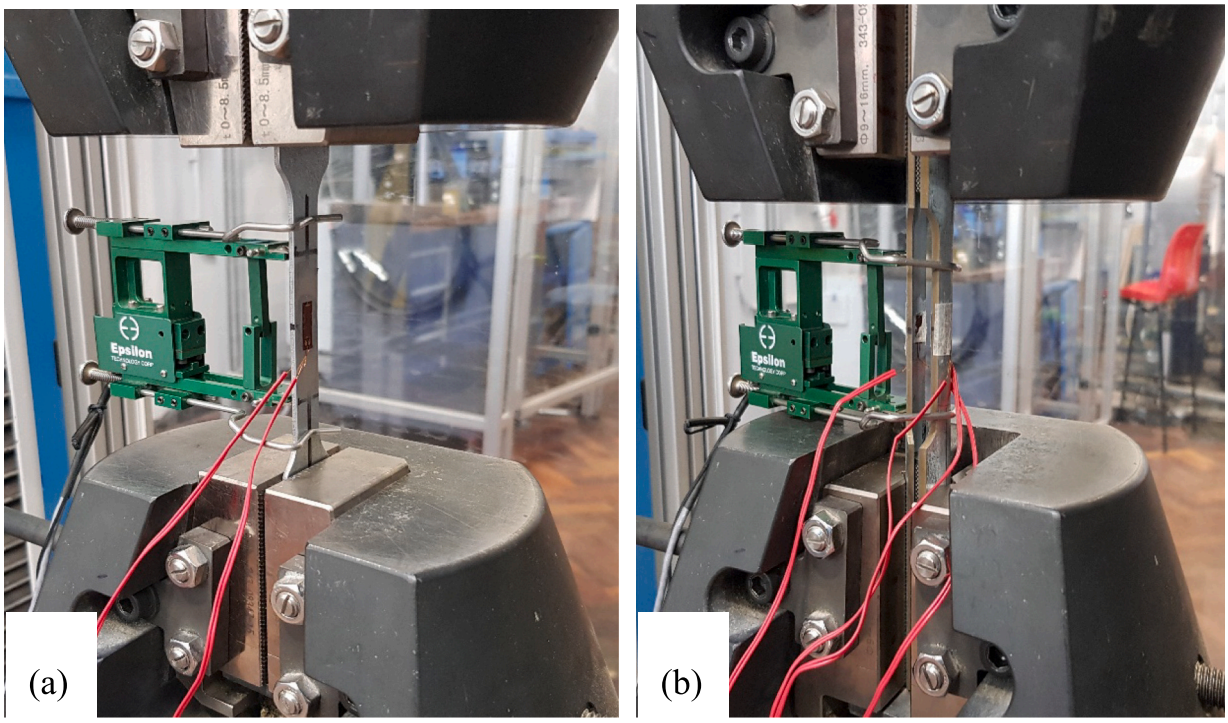

Fig. 3. Typical tensile test setup (a) flat specimens and (b) curved specimens.

mm/min. The stress-strain curves were then plotted, and the yield stress was calculated with an offset slope at strain level of 0.2%, while the initial Young's modulus, was determined by the readings obtained from strain gauges.

2.2. Predictive models

The influence of cold working on mechanical properties of curved regions of a cold formed section generally depended on some parameters such as: (1) the ratio of the ultimate tensile strength f_u to the yield strength f_y of the virgin material, (2) the ratio of the inner corner radius r to the thickness of the steel plate t, (3) the steel grade, (4) the type of manufacturing processes (roll forming or press-braking), (5) the type of stresses (compression or tension), and (6) the direction of stress with respect to the direction of cold working, i.e. transverse or longitudinal directions [2,25]. Among the above parameters, the ratios of f_u/f_y, r/t, and the type of manufacturing processes were the most important parameters to influence the change of material properties during manufacturing process. For instance, the effect of cold working on the enhancement of the yield strength increased when the ratio of f_u/f_y increased [2]. Small ratio of r/t, corresponded to a large degree of cold working in a corner which resulted the greater the enhancement in yield strength.

The material properties at corners and stiffener's bends were calculated from those of flat material by using analytical methods. One of the most popular methods was using formulae from the North American specification for the design of cold-formed steel structural members [2]. The equation for determining the tensile yield strength, f_{yc}, of the corner was based on Eq. (1). The Eqs. (1)–(3) are referred to hereinafter as specified in the AISI Specification [2].

$$F_{yc} = \frac{B_c F_{yv}}{\left(\frac{R}{t}\right)^m} \tag{1}$$

In which

$$m = 0.192\frac{F_{uv}}{F_{yv}} - 0.068 \tag{2}$$

$$B_c = 3.69\frac{F_{uv}}{F_{yv}} - 0.819\left(\frac{F_{uv}}{F_{yv}}\right)^2 - 1.79 \tag{3}$$

where: F_{yv} is the yield stress, F_{uv} is the ultimate strength of the material in flat parts of the section R is inside radius of the corner and t is the thickness of the section.

Gardner et al. [27] modified the AISI predictive model [Eqs. (2), (3)] using test results on corners of cold-formed steel box sections. The modified predictive model had revised values for coefficients, as shown in Eqs. (4), (5). Their predicted yield strengths were more accurate and consistent than those of the AISI predictive model for rectangular and square hollow sections.

$$m = 0.23\frac{F_{uv}}{F_{yv}} - 0.041 \tag{4}$$

$$B_c = 2.9\frac{F_{uv}}{F_{yv}} - 0.752\left(\frac{F_{uv}}{F_{yv}}\right)^2 - 1.09 \tag{5}$$

In this paper, the tensile test results obtained from tensile tests for section corners and stiffener bends were compared to the above two models and the results are presented in Section 5.2 to evaluate the predictive model's accuracy.

2.3. Bending tests

The typical test setup for the four-point bending configuration test of sections C-W145T1.2 and Z-W145T1.2 is shown in Fig. 4 (which shows the test setup of the channel sections). The beam sections were assembled in pair with lateral restraints made of 45 × 45 mm steel angles which were fixed by self-tapping screws to the top and bottom flanges at every distance of 500 mm, but there are no restraints on top of the sections for 1300 mm at the mid-span; this is to allow the distortional buckling failure in the beams. It was set up as simply supported beams

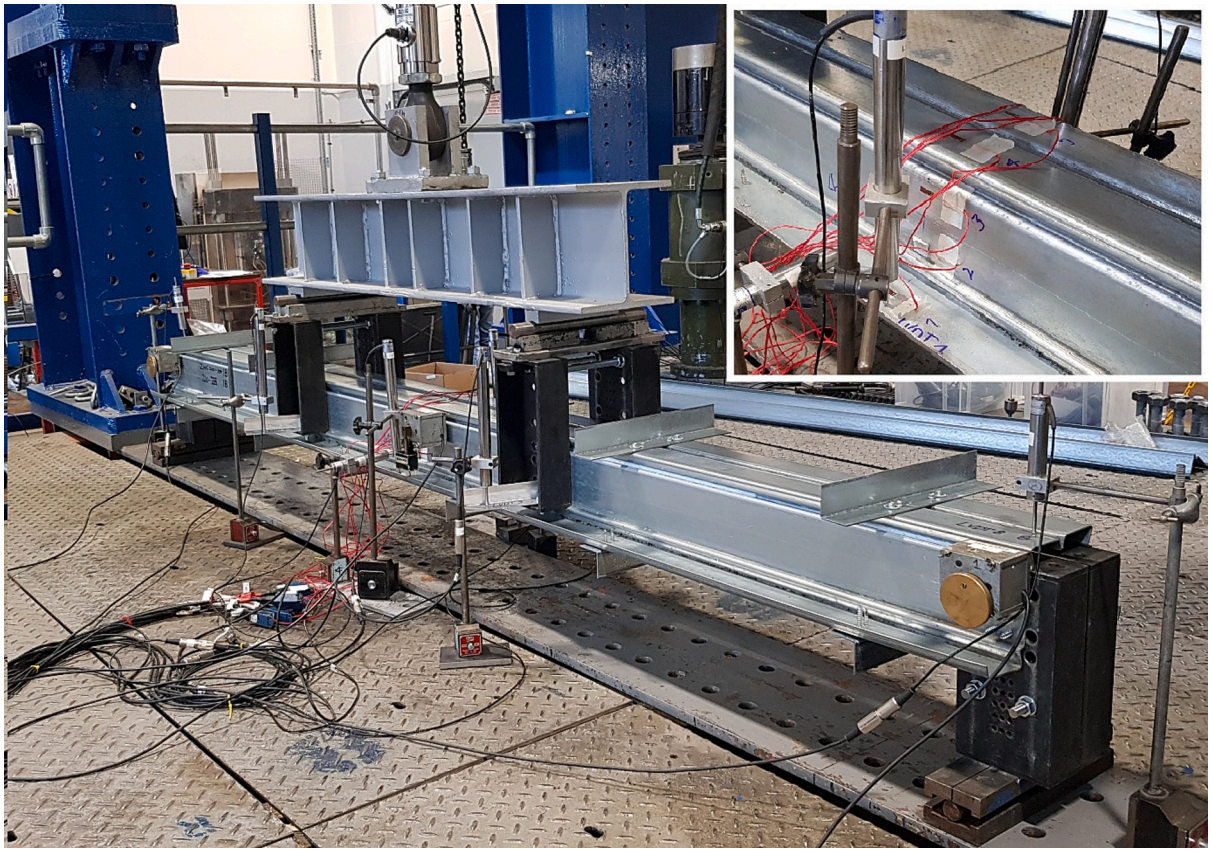

Fig. 4. Four-point bending test setup, showing zed sections and strain gauge and LVDTs arrangement at mid-span of the sections (in the small box).

which were supported on round blocks located 2700 mm apart.

A calibrated test rig was used for the tests which consists of a 200-kN capacity hydraulic actuator. It imposed the load through a rigid I beam onto the beam specimens at two discrete locations 900 mm apart. These loads were applied through the web of the section via a bolted connection using cleats (fixed to the beam webs), which in turn contacted the load cell beams via round blocks. Round blocks were used for all supports to ensure that the reaction force/ load applied to support cleats was a point load. Electrical strain gauges were used to measure the axial strains along the web and flanges of the cross section of the beam specimens. For each section, four strain gauges were mounted on the specimen mid-span, on the perimeter outside the specimen cross section, at the web positions close to the flanges and at the centres of flanges. Displacement transducers (LVDTs) were used for determining the vertical displacements under the beams at mid-span and under the two loading points. Other LVDTs were placed at the supports to measure possible displacement in the vertical direction.

A displacement control scheme with a rate of 1 mm/min was used for all tests. The specimens were loaded to failure. The tests stopped when the load dropped approximately 30% after reaching the maximum value. The data associated with load, displacement and strain gauge readings were recorded by data acquisition software. To consider the variation in sample and testing conditions, 2 duplicated tests were carried out for each section referenced.

3. Finite Element modelling and optimisation

3.1. FE modelling of four-point beam bending test

FE modelling was performed using ANSYS (Version 2020R, ANSYS, Inc.) to model the four-point bending test of the channel and zed sections, as presented in Section 2. The method of developing the FE model for thin-walled sections capable of simulating the buckling and ultimate strength while considering the section's geometric imperfections and cold working effects was presented in detail in Qadir et al. [12], and this method was applied to this study. The FE model setup including point load locations and boundary conditions is illustrated in Fig. 5 where only half of the test system was simulated due to symmetry (the tested beams had a span of $L = 2700$ mm, distance between two bracings at the end of beams is $a = 500$ mm, and distance between two bracings at the centre of beams is $b = 1300$ mm). The bracings were modelled using tie nodes at the symmetry plan that were rigidly connected to nodes from the top / bottom flanges and they were constrained to prevent from movement against the transverse direction.

The distance between two bracings at the centre of beams is approximately equal to three distortional buckling halfwave length of the sections [40]. The connections of support cleats attached to the web of the section at supports and loading points were also modelled by rigid connections between reference nodes (at centre of support) and nodes at screw positions. These reference nodes were used to restrict the section ends against all the movements such as vertical, transverse and out-of-plan rotations. The reference nodes at one-third of the beams were used to apply vertical loads.

The FE modelling of the beam test included two steps. In the first step, a linear elastic buckling analysis was performed on the perfect geometry to obtain distortional buckling modes (eigenvalues). In the second step, these buckling modes were used as initial geometric imperfections for a nonlinear post-buckling analysis carried out to predict the beam behaviour and ultimate load capacity. A linear elastic buckling analysis was carried out using FE method to obtain the dominant buckling modes (Eigenmodes), which were then fed into the nonlinear analysis to include the shape and distribution of initial imperfections. The distortional buckling mode, characterized by two half-waves along the constant moment span, was generally the primary mode in this study.

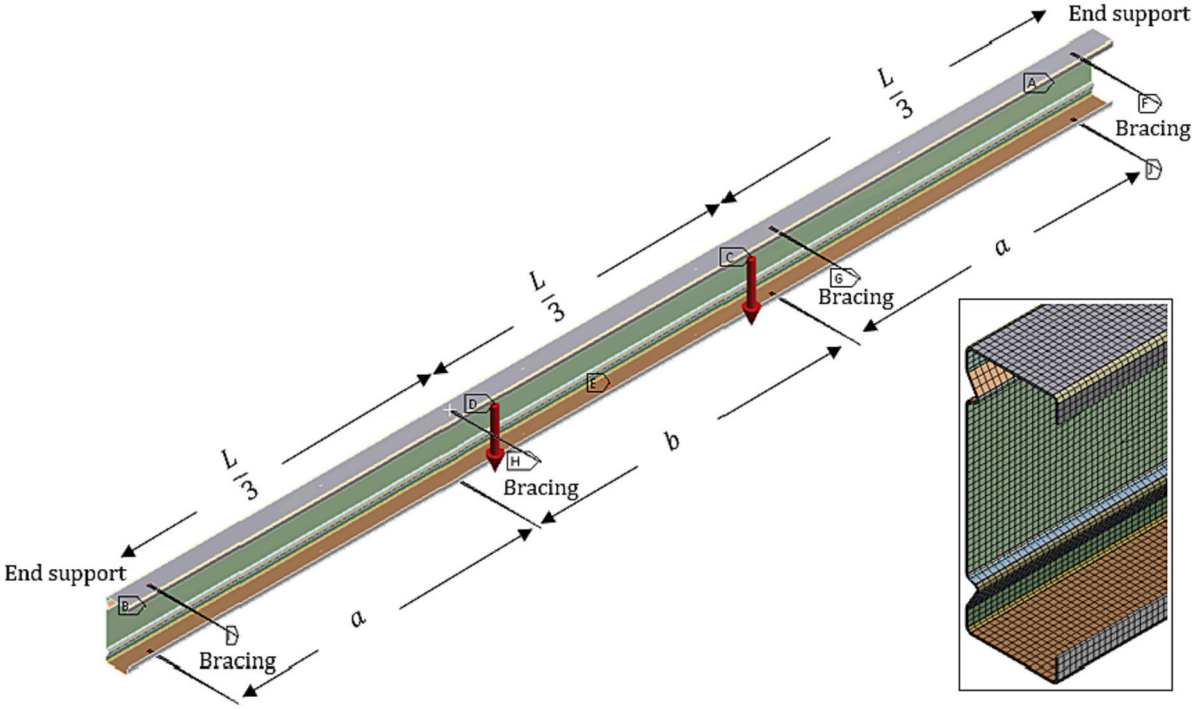

Fig. 5. FE model setup which shows boundary conditions (an example of the channel section is presented) and the mesh of the section in closer view, as shown in the rectangular box. $L = 2700$ mm, $a = 500$ mm, $b = 1300$ mm.

Shell elements SHELL181 which has 4-noded quadrilateral, reduced integration, were selected. There were two layers with 6 integration points through the thickness of the section, since the plastic deformation and shear deformation effects were considered in this study, the high number of integration points was preferred. These elements had three translational and three rotational degrees of freedom at each node that consider finite membrane and large rotations that are suitable for large-deformation and geometrically non-linear issues in this study. The material properties for flat parts, section corners and stiffener bends obtained from tensile tests (as presented in Section 2.1) were assigned in these regions of the channel section C-W145T1.2 and zed section Z-W145T1.2 in the FE models, as shown in Fig. 2. This allowed the effects of cold working on tensile and flexural strengths of cold rolled steel sections with complex stiffeners to be investigated. The value of 205 GPa was used elastic modulus E of steel material.

Four different mesh sizes were used to study the influence of the mesh parameter on the accuracy of the simulation results. They included sizes of 20 × 20 mm, 8 × 8 mm, 4 × 4 mm, and 2 × 2 mm, which corresponded to a total number of elements of 5694, 21,900, 70,810 and 233,600, respectively. The results showed that maximum difference between the ultimate loads of the 20 × 20 mm and the 2 × 2 mm was less than 5%. Using mesh sizes smaller than 4 × 4 mm has negligible effects on the stiffness and ultimate load capacity values (less than 0.5% difference), while could significantly increase the computational costs. Consequently, the 4 × 4 mm mesh size was chosen in this study to strike a balance between accuracy and computational efficiency. This choice ensured that simulation results aligned well with experimental findings while being sufficiently small to accurately model the corners and bends of the section's stiffeners.

To validate the FE results, the first buckling mode was compared with experimental observations, and a close resemblance was identified. Consequently, the first buckling mode shape was chosen for generating imperfections. The maximum amplitude of this mode shape served as a measure for the degree of initial imperfection. Past research has demonstrated that utilizing the first buckling mode shape derived from the elastic buckling analysis, in conjunction with appropriate initial geometric imperfections, yields accurate predictions for failure mode and strength capacity in the FE model.

The imperfection value of 1.55t was employed for the FE analysis in this study as suggested in [12] (using the imperfection value of 1.55t in the FE analysis was found to provide the closest agreement in the initial stiffness and strength values compared to the experimental results with less than 1% difference). More detailed information about the FE modelling can be found in Qadir et al. [12].

In this paper, the measured material properties obtained from tensile specimen tests for flat and corners/bends were used in the FE models to accurately quantify the effects of geometry and the cold working induced from the cold roll forming process. Figs. 9(a),(b) show the measured engineering stress-strain curves. The true stress-strain curves were determined using the following equations:

$$\sigma_{true} = \sigma_{eng}\left(1 + \varepsilon_{eng}\right) \tag{6}$$

$$\varepsilon^{pl}_{true} = ln\left(1 + \varepsilon_{eng}\right) - \frac{\sigma_{eng}}{E} \tag{7}$$

where σ_{eng} and ε_{eng} are engineering stress and strain, respectively, based on the original cross-section area of the tensile specimen; and σ_{true} and ε^{pl}_{true} are the true stress and the true strain, respectively, considering the actual cross-section area of the tensile specimen during the test.

While residual stresses were not directly included in the FE models, they were indirectly considered through the stress-strain data obtained from the material tests. Previous studies indicated that the membrane residual stresses can be safely ignored in the open sections [41,42]. On the other hand, longitudinal flexural residual stresses were implicitly represented in the stress-strain behaviour of the coupon tensile test results, given that the coupons were cut from the final sections.

It is noteworthy that cutting a coupon might release flexural residual stresses, causing the coupon to curl [21]. However, these stresses were reintroduced when the coupon was straightened during the initial stages of tensile loading. Consequently, the effects of residual stresses were not individually incorporated into the FE models but were assumed to be inherently included within the stress-strain data.

4. Flexural strength optimisation

This session study used the material properties obtained from the tensile test conducted in Section 2.1 (results presented in Section 5.1) in the FE models to optimise the buckling and ultimate strength of the associated channel and zed sections. Therefore, the effects of cold working on material properties at section's corners and stiffener bends on the flexural strengths could be evaluated from the experimental data. The optimisation was carried out for channel and zed sections with flange's stiffeners to evaluate the effectiveness of including intermediate stiffeners in the section flanges. The main purposes were to (1) accurately quantify both geometry and the cold working effects on the buckling and ultimate strength in the channel and zed sections with complex stiffeners, and (2) ultimately select and propose the optimal design of the channel and zed sections with both web and flange's stiffeners.

Two sets of channel and zed sections with the depth of 145 mm and thickness of 1.2 mm, and the depth of 170 mm and thickness of 1.6 mm were used for the optimisation work. They were the industrial UltraBeam™[2] and UltraZED™[2] sections, respectively (Hadley Industries plc.) that already had two longitudinal stiffeners on the web as shown in Fig. 1. The sections with the depth of 145 mm had tensile tests and bending tests presented in Sections 2.1 and 2.2, and results presented in Sections 5.1 and 5.2 in this paper. The sections with the depth of 170 mm and thickness of 1.6 mm had tensile tests conducted by the same procedure (results are not presented) and results were used for optimisation in this section. Material properties were not the same for the two sets of section depths so that the variation in the section strengths due to different material properties was studied in the design optimisation. These sections were defined as "reference" sections. For comparison purposes, channel and zed sections which were "reference" sections but had no web and flange stiffeners were also used in FE analysis, and they were referred as "standard" sections.

Figs. 6 and 7 shows general dimensions for the channel and zed sections, respectively, used in the optimisation. The FE model validated for bending tests in Section 2.2 (validation results were shown in Section 5.2) was utilised for the optimisation study in this paper. In the FE models of the "reference" channel and zed sections, the material properties for flat parts, section corners and stiffener bends obtained from tensile tests were assigned in these regions of the sections, as shown in Fig. 2. When the section included intermediate stiffeners in the flanges, the material properties for the section corners at position 3 were used for the region of the flange stiffener.

In the FE models of the sections used for optimization, except the section height h and thickness t were fixed, all dimensions were parameterized from p_1 to p_{17} as shown in Figs. 6 and 7. For example, Fig. 6(c) illustrates the channel section with flange stiffeners and all dimension parameters used for parametric study and optimisation. Parameters for the positions of the web stiffeners from the web-flange corner were p_1 and p_2 and the position of the peak of the web stiffeners in horizontal direction from the web-flange junction is p_3. Parameter p_4 was the width of the edge stiffener, parameter p_5 was the radius of the section corners (assuming all section corners had the same radius), parameters p_6 and p_7 were the angle of the web stiffener, parameter p_8 was the flange width, parameter p_{15} was the position of the flange stiffener from web flange junction in vertical direction, and parameters p_{16} and p_{17} were the size of the flange stiffener which was the radius of a circular stiffener.

The FE simulations conducted for each reference section ranged between 250 and 300 simulations. Taking C-W145T1.2 as an example, a total of 270 combinations were explored for parameters p_1, p_2, p_3,p_4,p_5, p_6, and p_7, considering values between lower bound of 1.00 mm and upper bound of 40.53 mm for p_1 and p_2, lower bound of 5.61 mm and upper bound of 23.61 mm for p_3, lower bound of 2.90 mm and upper bound of 7.50 mm for p_5, lower bound of 0^o and upper bound of 20^o degrees for p_6 and lower bound of 340^o degrees and upper bound of 360^o degrees (equivalent of 0^o) for p_7. Buckling load and flexural strength values, accounting for the cold working effect, were obtained for each parameter variation. The results were systematically compared to investigate the influence of these parameters. Table 1 lists the ranges of values considered for the optimisation of channel and zed sections.

The optimal cross-sectional shapes investigated in this paper, are optimised based on an optimisation framework developed by the

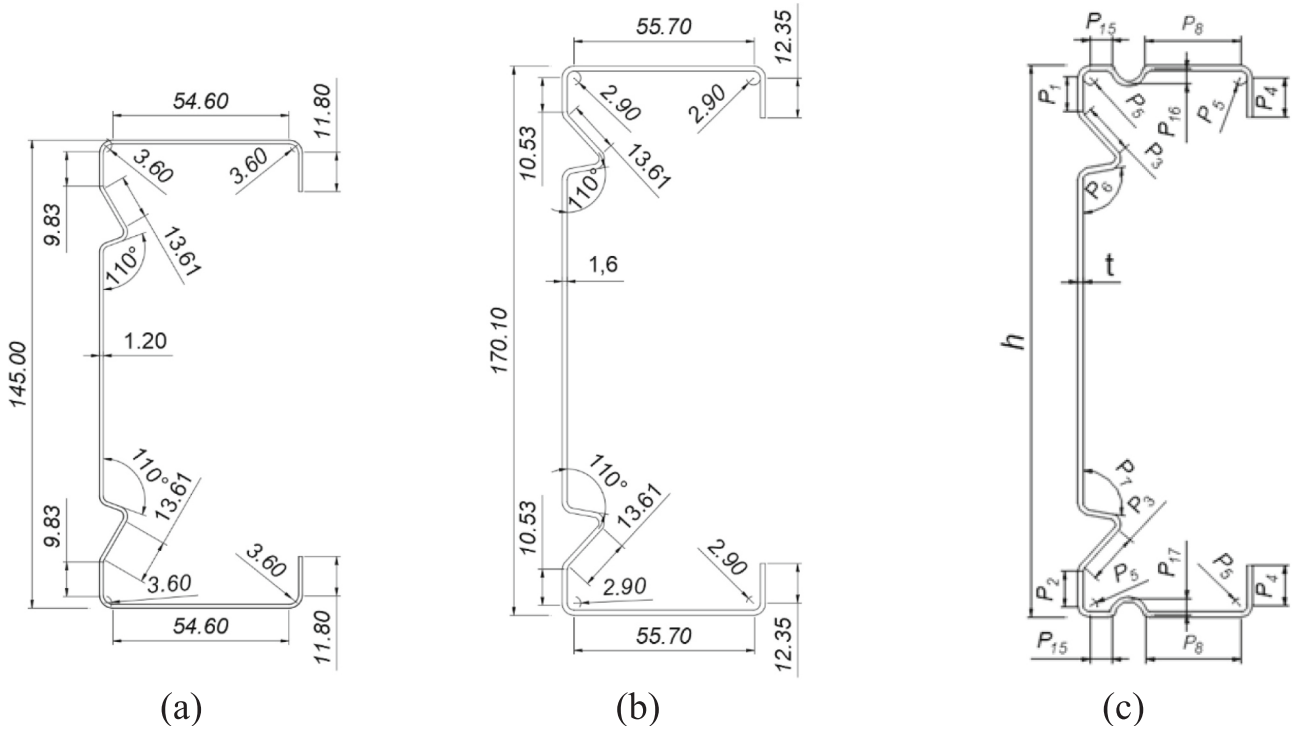

Fig. 6. Dimension parameters in (mm) and definition of design variables of the channel cross section (a) reference section h = 145 mm, (b) reference section h = 170 mm, and (c) section with geometric parameters used for optimisation.

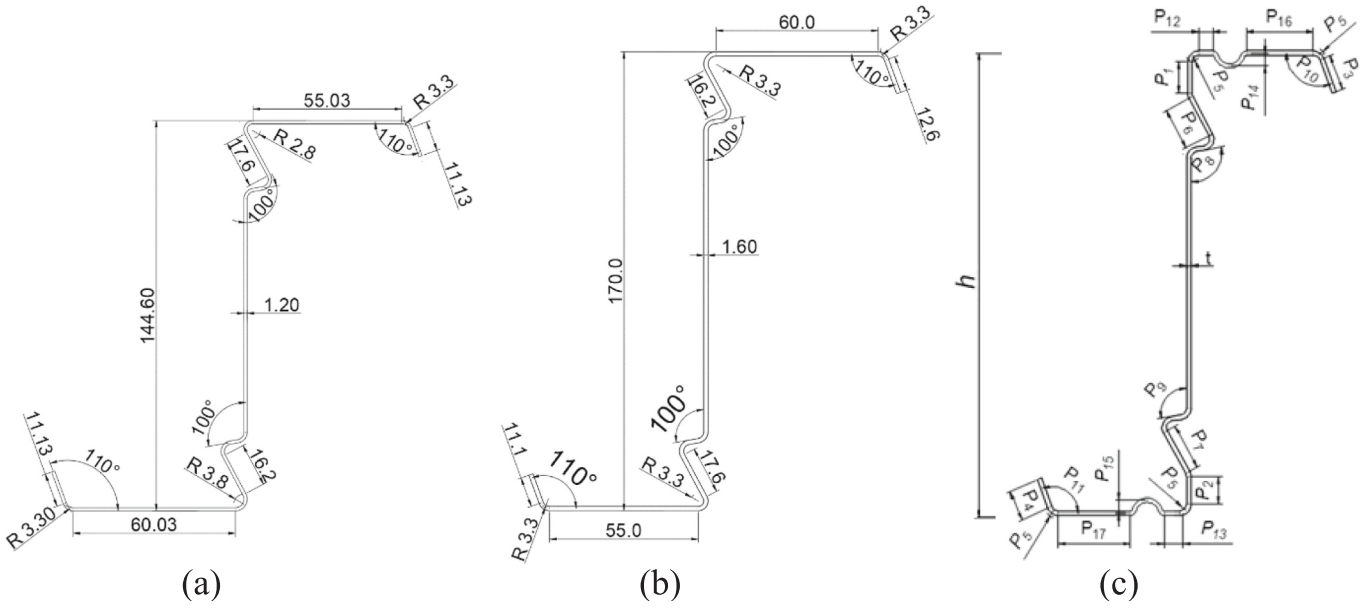

Fig. 7. Dimension parameters in (mm) and definition of design variables of the zed cross section (a) reference section h = 145 mm, (b) reference section h = 170 mm, and (c) section with geometric parameters used for optimisation.

Table 1
Ranges of values considered for the optimisation process (in mm for length parameters and degrees for angle parameters).

Parameter	Lower bound	Upper bound	Parameter	Lower bound	Upper bound
Channel section without flange stiffeners			Channel section with flange stiffeners		
p_1	1.0	40.5	p_1	1.0	40.5
p_2	1.0	40.5	p_2	1.0	40.5
p_3	5.6	23.6	p_3	5.6	23.6
p_4	12.4	18.4	p_4	12.4	18.4
p_5	2.9	7.5	p_5	2.9	7.5
p_6	0°	20°	p_6	0°	20°
p_7	340°	360°	p_7	340°	360°
–	–	–	p_{15}	5.0	20.0
–	–	–	p_{16}	1.0	5.0
–	–	–	p_{17}	1.0	5.0
Zed section without flange stiffeners			**Zed section with flange stiffeners**		
p_1	1.0	50.0	p_1	1.0	50.0
p_2	1.0	50.0	p_2	1.0	50.0
p_3	12.6	24.6	p_3	12.6	24.6
p_4	11.1	23.1	p_4	11.1	23.1
p_5	3.3	3.3	p_5	3.3	3.3
p_6	11.2	21.2	p_6	11.2	21.2
p_7	12.6	22.6	p_7	12.6	22.6
p_8	0.0°	30°	p_8	0°	40°
p_9	0.0°	30°	p_9	0°	40°
p_{10}	0.0°	20°	p_{10}	0°	20°
p_{11}	0.0°	20°	p_{11}	0°	20°
–	–	–	p_{12}	5.0	20.0
–	–	–	p_{13}	5.0	20.0
–	–	–	p_{14}	1.0	5.0
–	–	–	p_{15}	1.0	5.0

authors in the previous studies [10] for the purpose of producing more efficient and optimal design of CFS sections. The proposed optimisation framework takes the buckling and ultimate strength of CFS sections as objective function. A nonlinear FE model was first developed for referenced channel and zed sections under four-point bending tests. These reference sections were then parameterised utilising the Design Of Experiment (DOE) technique in terms of geometric dimensions and material properties and the section's distortional buckling and ultimate strength were determined.

Design of Experiments (DOE) is a methodology employed for planning experiments and gathering information to analyse the impact of input parameters on output parameters. The DOE technique involves conducting a series of experiments, systematically and simultaneously varying multiple experimental parameters. During each experiment, input variables are intentionally modified in a series of runs or tests, and data is collected to identify the process conditions and product components influencing the investigated quantities. The goal is to determine factor settings that optimise the objective responses. For more detailed information about DOE were described in [43].

In the following step, the effects of the stiffener's geometry including its location, shape, size, and material properties by the cold working at the section corners and stiffener bends on section strengths were expressed through a response surface. In general, Response Surfaces (RS) are defined as functions in which the output parameters are described in terms of the input parameters. In this study, the sampling points obtained from DOE method for one reference section were used to construct a Response Surface, which combined DOE method and mathematical statistics, continuously testing the specified points until the relationship between the input parameters was determined. The constructed Response Surface served to approximate target parameters in a global design space by estimating the set of input parameters, ultimately yielding an optimal response.

By applying an optimisation technique on these response surface data, optimal design of sections was determined based on the section's maximum ultimate strengths. For optimisation target, that was "obtaining maximum strength of the section while maintaining the same weight", the total length of the cross section was kept unchanged when changing all other dimension parameters. This process resulted in generating new channel and zed shapes.

In the proposed FE approach, as summarised in Fig. 8, a three-dimensional model of the section beams was built first, allowing for all section and stiffeners' dimensions to be parameterised as explained above. Next, the linear buckling analyses involved a two-step process. In the first step, a linear static analysis was formed in which unity point loads were applied at the loading points of the beam member. This initial step was necessary to calculate the internal stresses of the mesh and construct the geometric stiffness matrix of the beam structure (a linear perturbation). In the second step, an eigenvalue buckling analysis was carried out based on the formed geometric matrix to solve for

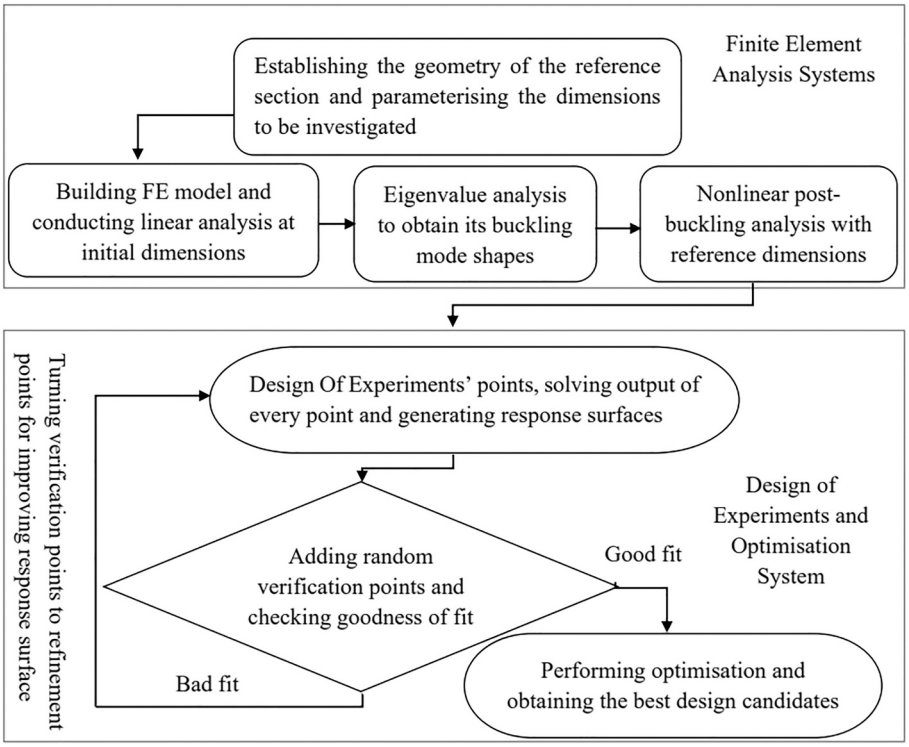

Fig. 8. The flowchart of the FE modelling and optimisation processes [13].

eigenvalues or linear buckling modes (the purpose of eigenvalue analysis is to investigate singularities in the linear perturbation of the beam's stiffness matrix).

The nonlinear buckling analysis was then carried out in which the initial imperfections, geometry and material nonlinearity were considered, including material properties changed at section corners and stiffeners' bends due to the cold working effect. This setup was linked together, allowing the three analysis systems to share resources from the first step "linear buckling analysis" such as engineering data, geometry, and boundary condition type definitions. Finally, the response surfaces were calculated using the data from the parameterised DOE process, and by using a multi-objective genetic algorithm, the optimal design candidates could be selected. The detailed descriptions of the optimisation approach could be found in [13].

The dimensions of the standard (sections have no web and flange stiffeners), reference (tested sections) and the cross-sections with parameters used for optimisation are presented in Tables 2–3. All the dimensions in the Tables are defined based on the mid-surface line. The "reference" cross sections provided a basis for comparison. Reference (b) and (c) are the "reference" sections without and with flange stiffeners, respectively. Candidates 1, 2 and 3 are optimised sections developed from both Reference (b) section, and Candidates 4, 5 and 6 are optimised sections developed from both Reference (c) section, in which they were obtained based on different target objectives. They were as follows:

- Candidates 1 of Reference (b) and Candidate 4 of Reference (c) were obtained when the optimisation target was to minimise the flexural developed stresses in the sections. The expression of "minimise the flexural developed stresses" means obtaining the maximum flexural strength based on minimising the flexural stresses in the sections (Usually, the structure gains maximum bending moment capacity when the bending stress is minimum).
- Candidates 2 of Reference (b) and Candidate 5 of Reference (c) were obtained when the optimisation target was to maximise the buckling loads in the sections. The expression of "maximise the buckling loads" means obtaining the maximum flexural strength based on maximising the buckling load of the section (Usually, the structure gains maximum bending moment capacity when the buckling capacity is maximum).

Table 2
Cross-sectional dimensions of standard, reference, and optimised channel sections.

Parameter	Standard	Reference		Candidate					
		(b)	(c)	1	2	3	4	5	6
p_1 (mm)		10.50	10.50	1.00	1.00	1.00	1.00	1.00	1.00
p_2 (mm)		10.50	10.50	1.00	1.00	1.00	1.00	1.00	1.00
p_3 (mm)		13.60	13.60	19.00	19.00	19.00	14.40	22.00	16.00
p_4 (mm)	12.30	12.30	12.30	16.00	18.00	17.00	13.50	18.00	13.10
p_5 (mm)	2.90	2.90	2.90	2.90	2.90	2.90	2.90	2.90	2.90
p_6 (degree)		0.00	0.00	15.00	15.00	15.00	15.00	15.00	15.00
p_7 (degree)		360.00	360.00	345.00	345.00	345.00	345.00	345.00	345.00
p_8 (mm)	62.00	55.70	35.20	43.50	41.5	42.50	28.70	23.00	28.00
p_{15} (mm)			5.00				5.00	5.00	5.00
p_{16} (mm)			5.00				5.00	5.00	5.00
p_{17} (mm)			5.00				5.00	5.00	5.00

Table 3
Cross-sectional dimensions of standard, reference, and optimised zed sections.

Parameter	Standard	Reference		Candidate					
		(b)	(c)	1	2	3	4	5	6
p_1 (mm)		0.00	0.00	0.00	0.00	0.00	0.00	0.00	0.00
p_2 (mm)		0.00	0.00	0.00	0.00	0.00	0.00	0.00	0.00
p_3 (mm)	12.60	12.60	12.60	19.70	17.70	20.80	17.00	19.00	18.40
p_4 (mm)	11.10	11.10	11.10	17.50	16.40	17.80	16.00	17.00	16.20
p_5 (mm)	3.30	3.30	3.30	3.30	3.30	3.30	3.30	3.30	3.30
p_6 (mm)		16.20	16.20	12.50	21.00	11.60	12.00	13.00	12.80
p_7 (mm)		17.60	17.60	13.90	21.00	12.90	13.00	14.00	13.10
p_8 (degree)		0.00	0.00	0.00	0.00	0.00	0.00	0.00	0.00
p_9 (degree)		0.00	0.00	0.00	0.00	0.00	0.00	0.00	0.00
p_{10} (degree)		20.00	20.00	0.00	0.00	0.00	0.00	0.00	0.00
p_{11} (degree)		20.00	20.00	0.00	0.00	0.00	0.00	0.00	0.00
p_{12} (mm)	68.60	60.00	5.00	51.00	44.00	51.00	5.00	5.00	5.00
p_{13} (mm)	63.00	55.00	5.00	46.00	39.00	46.00	5.00	5.00	5.00
p_{14} (mm)			5.00				5.00	5.00	5.00
p_{15} (mm)			5.00				5.00	5.00	5.00
p_{16} (mm)			39.30				35.80	33.70	35.50
p_{17} (mm)			34.30				30.70	28.80	29.00

- Candidates 3 of Reference (b) and Candidate 6 of Reference (c) were achieved when the optimisation target was to minimise the flexural developed stresses and maximise the buckling loads in the cross sections.

It should be noted that it is not practical and not preferred to set the ultimate load as the objective function for the optimisation process due to the following reasons: (1) the nonlinear analysis was usually failed when the elements were exhibiting large plastic deformation or closely reaching the ultimate load due to numerical non-convergence issues, which meant using the final load value as the ultimate load might not be accurate, (2) achieving accurate ultimate load values would require continual fine-tuning of nonlinear analysis settings for each section. This involves adjustments to mesh size, increment size, iterative solution, constrained solution (arc-length), convergence criteria, etc. Given the repetitive nature of this process, it's not feasible to apply it to all analyses for the multitude of optimised sections, about 2400 simulations for all sections.

To address the above issue, this study employed a practical optimisation approach. Structures typically attain maximum bending moment capacity either when buckling capacity is at its peak or when bending stress is minimised. Linear buckling analysis was employed to achieve the former, while the latter was determined through nonlinear analysis at the applied load value just before reaching ultimate strength and failure. For instance, in the optimisation process for channel C-W145T1.2 and zed Z-W145T1.2, various applied load values between 22 and 25 kN were tested. However, 24 kN was chosen for this study, as most sections could withstand this load level just before reaching ultimate strength and failing. After identifying an optimal section based on these objective criteria, nonlinear analysis of these sections was conducted. This involved further refining settings such as mesh size, increment size, iterative solution, constrained solution, and convergence criteria to accurately determine the section's ultimate strength. For a more detailed explanation of this method, refer to [12,13].

When an optimal section was found based on these objective criteria, the nonlinear analysis of these sections was then conducted with refined settings of mesh size, increment size, iterative solution, constrained solution, and convergence criteria to accurately achieve the section's ultimate strength. The detailed description of this method could be found in [12,13]. In this study, the sections were optimised based on the three target objectives using the method mentioned above. During the optimisation process, it was observed that the optimised sections tend to have the minimum flexural developed stresses due to an increase in the sectional modulus of the sections (Candidates 1 of Reference (b) and Candidate 4 of Reference (c)). The optimised sections also tend to have the maximum buckling loads in the sections due to a decrease in the distortional buckling slenderness (Candidates 2 of Reference (b) and Candidate 5 of Reference (c)).

These two combinations ultimately enhanced the ultimate load capacity of the sections, with the exception of a certain limit observed in Candidates 2 and 5. While these candidates considerably improved distortional buckling capacities for channel and zed sections, they had a limited effect on ultimate moment capacity and actually led to noticeable reductions in Candidates 2 and 5 compared to Candidates 3 and 6. This reduction was attributed to a significant decrease in the sectional modulus in the minor axis, making these sections more susceptible to failure due to distortional-global interaction buckling and consequently resulting in lower ultimate moment capacities for the beam sections. These findings align with observations from previous studies [12,13].

5. Results and discussion

5.1. Tensile test results

The key measured material properties (static engineering values) obtained for flat and curved specimens are listed in Table 4, where f_y is the 0.2% proof stress, f_u is the ultimate tensile strength, and ε_f is the elongation after fracture, measured over a gauge length of 50 mm. Table 4 shows that the material properties of measured flat specimens cut from the web and flange were similar. These were consistent with results from previous studies [14,15]. However, the mechanical properties of section corners and stiffener bends significantly enhanced due to work hardening that arises from plastic deformations induced during

Table 4
Measured material properties of tensile specimen of channel section C-145 T1.2 and zed section Z-145 T1.2 (For flat specimens, the average result of three repeated tests a, b, c was presented; for corner specimens, the average result of two repeated tests a, b was presented).

Section	Type	Region	f_y (N/mm^2)	f_u (N/mm^2)	ε_f (%)
Channel C-W145T1.2	Flat	Flange	488.72	562.88	17
		Web	500.46	568.00	16
	Corner	Position 1	522.53	621.03	6
		Position 2	554.29	618.06	7
		Position 3	549.98	585.48	6
Zed Z-W145T1.2	Flat	Flange	467.32	545.09	23
		Web	460.21	536.36	23
	Corner	Position 1	549.53	636.60	11
		Position 2	539.21	638.11	13
		Position 3	556.30	626.36	10

the cold roll forming process. Fig. 9 shows the static stress-strain curves of typical flat specimens and the pair of curved specimens taken from the sections C-W145T1.2 and Z-W145T1.2.

Stresses and strains shown in this figure are conventional engineering values. For the channel section, in comparison to the flat specimens, the yield and tensile strengths of the curved specimens were increased by 7–12% and 4–10%, respectively, and the percentage of elongation decreased by 60–70%. For the zed section, the yield and tensile strengths of the curved specimens were increased by 16–20% and 16–18%, respectively, and the percentage of elongation decreased by 43–57%. It confirmed that the cold working produced a significant increase in the yield and tensile strengths and a decrease in ductility of the section corners and stiffener's bends. The effect of the cold working on the mechanical properties of web and flange specimens, however, was very small, so that the difference could be neglected.

5.2. Comparisons of strength increase between measurement and predictive models

Table 5 shows values and comparisons between the yield stresses of the channel and zed section and stiffener corners measured from the experiments $f_{yc,test}$ and calculated using the predictive models (AISI [2] and Gardner et al. [27]) $f_{yc,predictive}$,. Overall, it can be observed that the measured yield stresses of the section and stiffener corners were greater than those of the flat materials (as presented in Table 4), with an average increase of 16%.

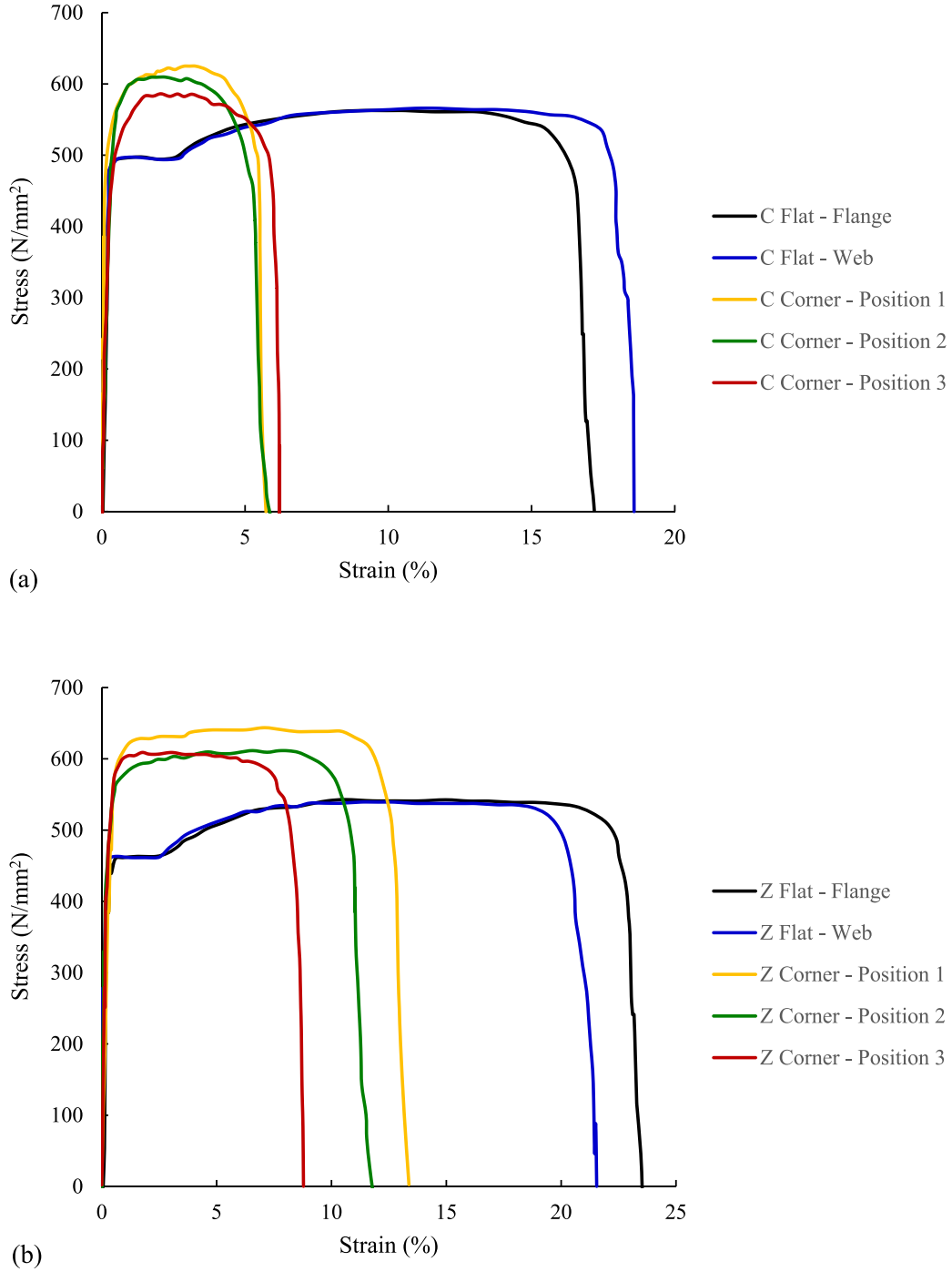

Fig. 9. Engineering stress–strain relationships of flat and corner specimens for (a) channel section C-W145T1.2, and (b) zed section Z-W145T1.2.

Table 5
Comparison of yield strengths obtained by the proposed predictive models and representative test data for the 0.2% proof strength of curved regions of cold-formed sections ($f_{yc,pred}/f_{yc,test}$). ①, ② and ③ stand for the postions 1, 2 and 3, respectivety.

Curved specimens (1)	Corner position (2)	Corner thickness (3)	$f_{yc,test}$ (4)	$f_{yc,predictive\ model}$		Comparison	
				AISI (5)	Gardner et al. [27](6)	(5)/(4) (7)	(6)/(4) (8)
C-W145T1.2	① $r = 3.18$	① $t = 1.23$	522.53	449.23	363.34	0.86	0.70
	② $r = 1.98$	② t = 1.23	554.29	489.21	410.17	0.88	0.74
	③ $r = 2.78$	③ $t = 1.24$	549.98	460.74	383.50	0.84	0.70
Z-W145T1.2	① $r = 2.38$	① $t = 1.12$	549.53	583.97	492.11	1.06	0.90
	② r = 2.38	② t = 1.12	539.21	582.69	490.57	1.08	0.91
	③ r = 2.78	③ t = 1.24	556.30	566.15	481.23	1.02	0.87
C-W170T1.6	① $r = 2.54$	① $t = 1.59$	539.50	615.05	525.99	1.14	0.98
	② $r = 3.15$	② $t = 1.55$	527.00	590.47	496.06	1.12	0.94
	③ $r = 3.48$	③ $t = 1.56$	515.00	581.23	481.23	1.13	0.94
Z-W170T1.6	① $r = 3.46$	① $t = 1.54$	550.00	578.14	478.66	1.05	0.87
	② $r = 3.47$	② t = 1.54	525.00	566.99	478.31	1.08	0.91
	③ $r = 3.47$	③ t = 1.55	500.00	567.61	487.76	1.14	0.98

For all the section and stiffener corner regions, the results obtained from both of the predictive models, the AISI Specification [2] and Gardner et al. [27], showed that the yield stresses were significantly enhanced in comparison with the flat material with an average increase of 22%. As illustrated in Table 4, in general, the measured yield stresses well correlated with the predicted values from the AISI specification with a maximum difference of ±16%. It showed that the AISI model predicted greater values of the yield stress in comparison with the measured values for more than 75% of data. However, there were few data (C-W145T1.2 specimens) that the AISI model predicted smaller values of the yield stress with a difference from 12% to 14%. On the other hand, the model proposed by Gardner et al. [27] generally under estimated the strength enhancement from 2% to 30%. As this model was mainly calibrated based on cold rolled hollow sections, the AISI model was more universally applicable and was thus recommended for predicting the yield strength at corners of cold-formed steel sections when test data was not available.

5.3. FE modelling of four-point beam bending test and validation

The FE models was carried out for four-point beam bending tests conducted in Section 2.2 and the results were compared with the experimental results to validate the models. The comparison of ultimate moment capacity for beams is summarised in Table 6, where M_u, M_{uc} stand for ultimate moment capacities for not considering and considering the true material properties by the cold working effect, respectively. It shows the FE results were in an excellent agreement with the experimental results for ultimate moment values. In addition, good comparison of experimental results and FE simulation models in terms of load-displacement curves is shown in Fig. 10 and Fig. 11. It was observed that the distortional buckling failure mode was well captured by the FE models in the deformed shapes of the channel section in Fig. 10 (b) and of the zed section in Fig. 11(b). In particular, the FE failure modes showed that the inward compressed flange-lip motion in post buckling state of the channel cross section was 20.73 mm at failure for the channel section; and it was 12.61 mm at failure for the zed section. This clearly indicated the distortional buckling mode of failure of these sections, and the zed sections were less prone to distortional buckling failure mode. The contours represented the displacement occurred in the section and noted that the red colour represented the maximum displacement, whereas as the colour became lighter the displacement became smaller values. It can be seen from Table 6 that the increase of flexural strength by assigning the true material properties at the section and stiffener's corners is small; it was about 1% for both channel and zed sections.

Table 6
Ultimate moment capacities obtained from experimental tests and FE models. M_u and M_{uc} stand for ultimate moment capacity without and with the cold working effect, respectively. The average value was presented for the test result.

Section	M_{test} (kNm)	FEM		M_{test}/M_u	M_{test}/M_{uc}
		M_u (kNm)	M_{uc} (kNm)		
Channel	5.32	5.58	5.64	0.95	0.94
Zed	5.60	5.87	5.94	0.95	0.94

5.4. Optimisation for flexural strength

Tables 7 and 8 show the buckling and ultimate strengths of the cross-sectional geometries obtained from the optimisation process for the two sets of channel and zed sections using the measured material properties from the tensile specimen tests. They are compared with the strengths of the standard sections with the same amount of material and the same section height. The resulting cross-sectional shapes and comparison between flexural strength capacities with the cold working effect and without the cold working effect, of all optimal design candidates, Candidates 1–6, are also shown in Figs. 12 and 13 for the two sets of channel and zed sections with the depths of 145 mm and 170 mm, respectively. Table 9 summarises the increase of flexural strengths of the reference and optimised sections in comparison to the standard sections in which the increase of flexural strengths in the sections with flange stiffeners is highlighted. It should be noted that the optimisation process found the optimal positions, shapes and dimensions for the web and flange's stiffeners as shown in Figs. 12 and 13 in which the position for the flange stiffener was the closest to web-to-flange corner.

The following observations were made from Tables 7, 8, 9 and Figs. 12, 13:

For channel sections with the depth of 145 mm:

- Adding two longitudinal stiffeners to the web of the sections (reference (b)) significantly increased the buckling load, by 33% when compared with the standard section. The enhancement in ultimate load was noticeably improved by 21%, but the cold working effect was not significant (less than 1%). When the section was optimised, the maximum increase of the buckling load was 65% (Candidate 2) while the maximum ultimate moment capacity was up to 32% (Candidates 1 and 3). The influence of the cold working was significant for Candidate 2 with a maximum increase of 5%, but it was insignificant for Candidates 1 and 3.
- Adding one longitudinal stiffener to the top and bottom flanges of the reference section (reference (c)) resulted in further enhancement in the section's strengths. The buckling load was increased by 55% when compared with the standard section, while the ultimate moment capacity was increased by 40% and when the cold working effect was included, the increase was a further 2%. When the section

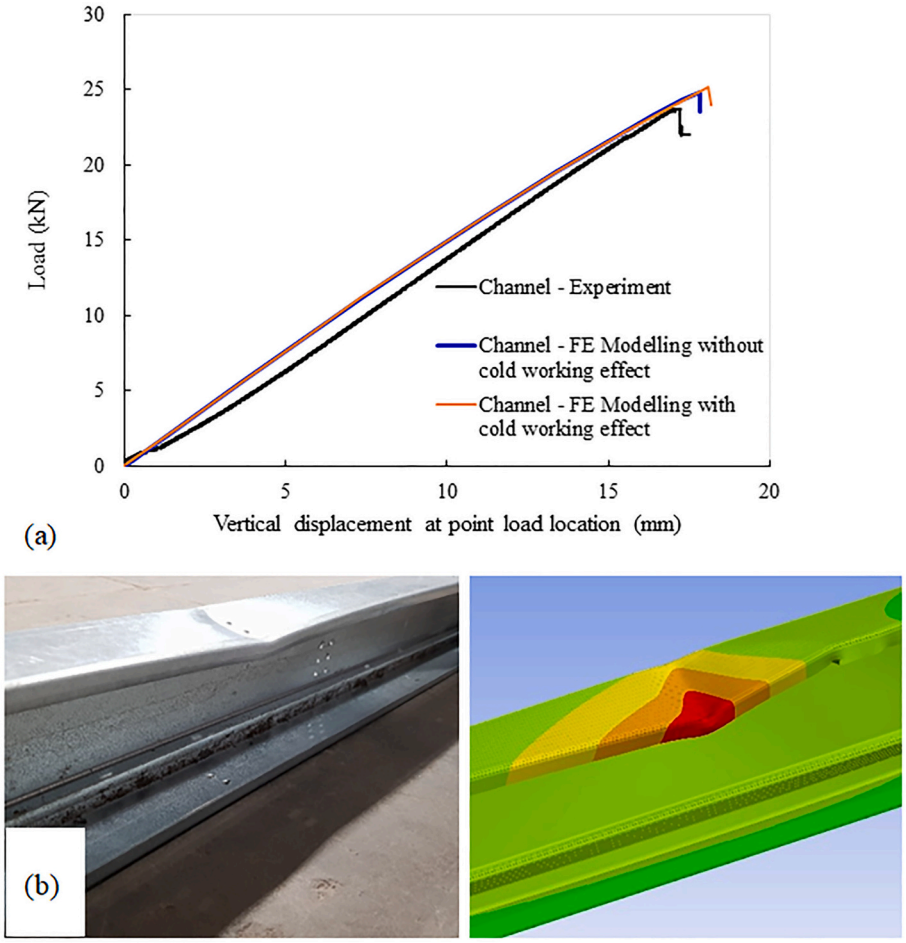

Fig. 10. Experimental and FE modelling results for channel section C-W145T1.2 (a) typical load-displacement curves, and (b) deformed shapes at failure from experiment and FE modelling (contour of displacement ranged from red to green with highest values in red region). (For interpretation of the references to colour in this figure legend, the reader is referred to the web version of this article.)

was optimised, the maximum increase of the buckling load was 131% (Candidate 5) while the maximum ultimate moment capacity was 50% (Candidate 4). The influence of the cold working was significant for Candidate 6 with a maximum increase of 5%, but it was 2–3% for Candidates 4 and 5.

For zed sections with the depth of 145 mm:

- Adding two longitudinal stiffeners to the web of the sections (reference (b)) significantly increased the buckling load, by 46% when compared with the standard section. The ultimate load enhancement was noticeably improved by 20%, but the cold working effect was less than 1%, which was not significant. When the section was optimised, the maximum increase of the buckling load was 50% (Candidate 2) while the maximum ultimate moment capacity was up to 23% (Candidate 2). The influence of the cold working was significant for Candidates 1 and 3 with a maximum increase of 9% (from 18% to 27%), but it was 3% for Candidate 2.
- Adding one longitudinal stiffener to the top and bottom flanges of the reference section (reference (c)) resulted in further enhancement in the section's strengths. The buckling load was increased by 60% when compared with the standard section, while the ultimate moment capacity was increased by 29% and when the cold working effect was included, the increase was a further 3%. When the section was optimised, the maximum increase of the buckling load was 75% (Candidate 5) while the maximum ultimate moment capacity was 36% (Candidate 4). The effect of the cold working was 2–3% for all Candidates 4, 5 and 6.
- Candidate 4 is the optimal solution, for both the channel and zed sections with the section depth of 145 mm which gained most increase in the buckling and ultimate moment capacities without the cold working effect, and with the cold working effect. They were 118%, 50% and 53% for the channel section, respectively, and 96%, 36% and 38% for the zed section, respectively.

For channel sections with the depth of 170 mm:

- Adding two longitudinal stiffeners to the web of the sections (reference (b)) significantly increased the buckling load, by 15% when compared with the standard section. However, the enhancement was not noticeable for the ultimate moment capacity with a maximum increase of less than 2%. For optimised sections, the maximum increase of the buckling load was 101% (Candidate 2) while the maximum ultimate moment capacity was 8% (Candidates 1 and 3). The influence of the cold working was significant for all Candidates 1, 2 and 3 with a maximum increase of 4%.
- Adding one longitudinal stiffener to the top and bottom flanges of the reference section (reference (c)) resulted in further enhancement in the section's strengths. The buckling load was increased by 31% when compared with the standard section, while the ultimate moment capacity was increased by 2% and when the cold working effect was included, the increase was a further 6%. For optimised sections, the maximum increase of the buckling load was 97%

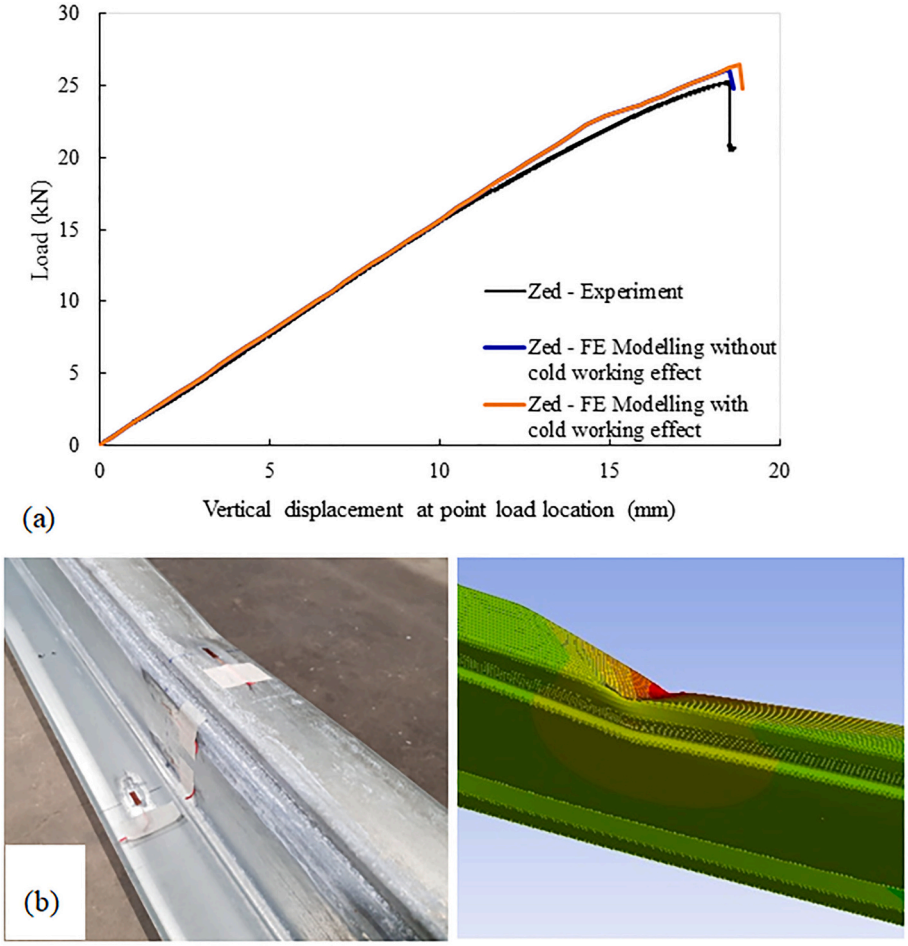

Fig. 11. Experimental and FE modelling results for channel section Z-W145T1.2 (a) typical load-displacement curves, and (b) deformed shapes at failure from experiment and FE modelling (contour of displacement ranged from red to green with highest values in red region). (For interpretation of the references to colour in this figure legend, the reader is referred to the web version of this article.)

Table 7
Buckling and ultimate moment capacity of standard and optimised channel and zed sections with the depth of 145 mm. M_u and M_{uc} stand for ultimate moment capacity without and with the cold working effect, respectively.

Section	P_b (kN)	M_u (kNm)	M_{uc} (kNm)	M_{uc}/M_u	$M_{uc}/M_{uc}^{standard}$
Channel					
Standard	4.90	4.58	4.68	1.02	1.00
Reference (b)	6.50	5.52	5.68	1.02	1.20
Candidate 1	6.70	6.10	6.17	1.01	1.30
Candidate 2	8.10	5.47	5.78	1.06	1.24
Candidate 3	6.70	6.10	6.17	1.00	1.30
Reference (c)	7.60	6.39	6.63	1.04	1.42
Candidate 4	10.70	6.86	7.17	1.05	1.53
Candidate 5	11.30	6.62	6.86	1.04	1.46
Candidate 6	11.00	6.65	7.02	1.05	1.50
Zed					
Standard	5.60	4.90	4.90	1.00	1.00
Reference (b)	8.20	5.81	5.87	1.01	1.20
Candidate 1	8.20	5.78	6.24	1.08	1.27
Candidate 2	8.40	6.03	6.17	1.02	1.26
Candidate 3	8.20	5.78	6.24	1.08	1.27
Reference (c)	8.90	6.33	6.45	1.02	1.32
Candidate 4	11.00	6.66	6.76	1.02	1.38
Candidate 5	9.80	6.47	6.61	1.02	1.35
Candidate 6	9.80	6.43	6.53	1.02	1.33

Table 8
Buckling and ultimate moment capacity of standard and optimised channel and zed sections with the depth of 170 mm. M_u and M_{uc} stand for ultimate moment capacity without and with the cold working effect, respectively.

Section	P_b (kN)	M_u (kNm)	M_{uc} (kNm)	M_{uc}/M_u	$M_{uc}/M_{uc}^{standard}$
Channel					
Standard	11.70	9.48	9.48	1.00	1.00
Reference (b)	13.40	9.48	9.63	1.02	1.02
Candidate 1	22.90	9.89	10.25	1.04	1.08
Candidate 2	23.50	9.62	9.87	1.03	1.04
Candidate 3	23.30	9.91	10.26	1.04	1.08
Reference (c)	15.30	9.67	10.26	1.07	1.08
Candidate 4	20.80	10.18	10.85	1.07	1.14
Candidate 5	23.10	10.31	10.96	1.07	1.16
Candidate 6	21.50	10.69	11.40	1.07	1.20
Zed					
Standard	9.60	9.03	9.03	1.00	1.00
Reference (b)	11.60	9.61	9.77	1.02	1.08
Candidate 1	19.70	10.38	10.55	1.02	1.17
Candidate 2	21.10	9.52	9.74	1.02	1.08
Candidate 3	20.20	10.52	11.11	1.06	1.23
Reference (c)	13.30	9.98	10.54	1.06	1.17
Candidate 4	18.80	10.38	10.91	1.05	1.21
Candidate 5	20.30	10.30	10.94	1.06	1.21
Candidate 6	19.80	10.52	11.11	1.06	1.23

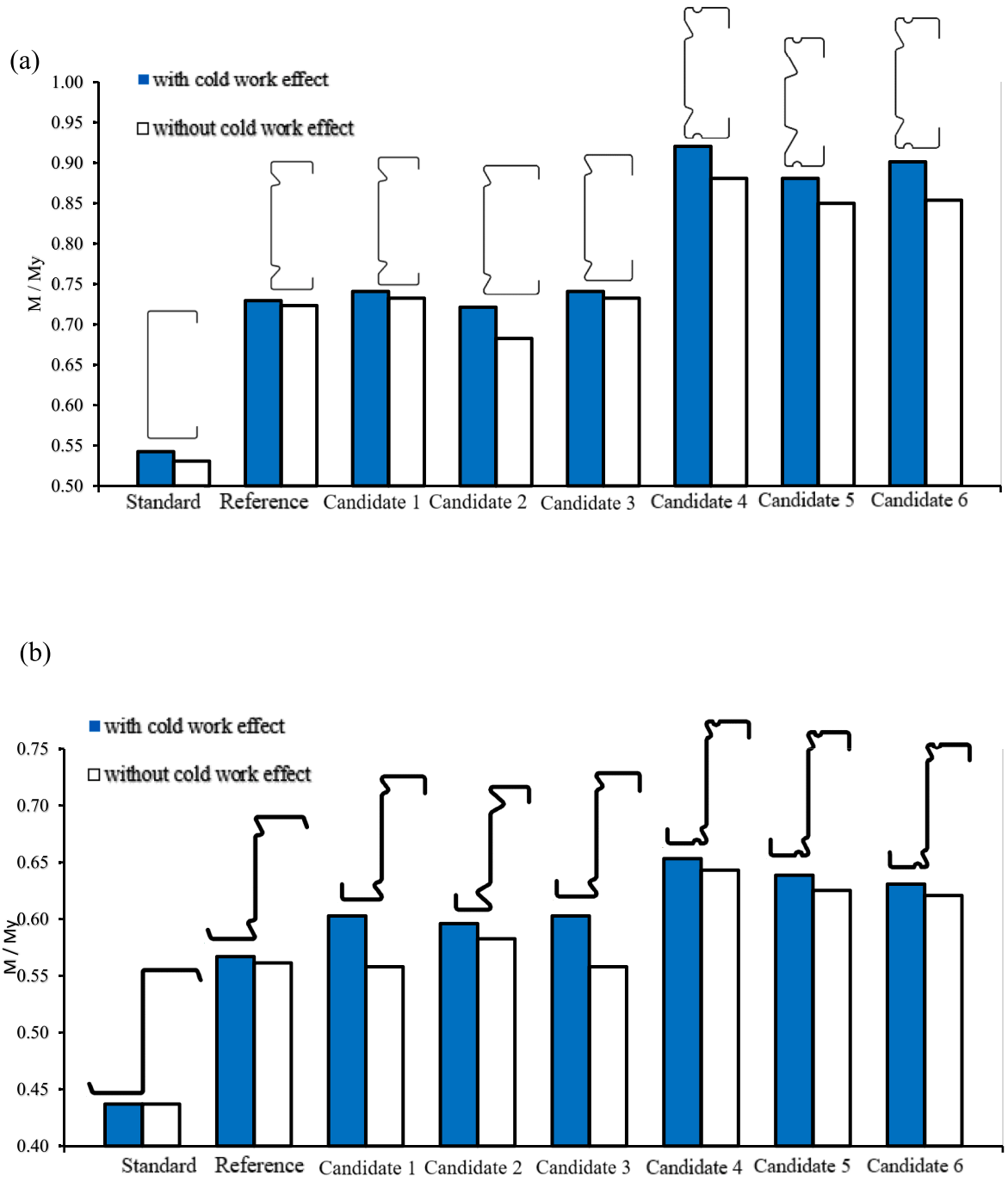

Fig. 12. Ultimate strength to yield ratio with the cold working effects and without the cold working effects for (a) channel cross sections with the depth of 145 mm, and (b) zed cross sections with the depth of 145 mm.

(Candidate 5) while the maximum ultimate moment capacity was 13% (Candidate 6). The influence of the cold working was significant for all Candidates 4–6 with a maximum increase of 7%.

For zed sections with the depth of 170 mm:

- Adding two longitudinal stiffeners to the web of the sections (reference (b)) significantly increased the buckling load, by 21% when compared with the standard section. The enhancement for the ultimate moment capacity was increased with a maximum of 6% and when the cold working effect was included, it was a further increase of 2%. The maximum increase of the buckling load for optimised sections was 120% (Candidate 2) while the maximum ultimate moment capacity was 15–17% (Candidates 1 and 3). The influence of the cold working was significant for Candidate 3 with a maximum increase of 5%.
- Adding one longitudinal stiffener to the top and bottom flanges of the reference section (reference (c)) resulted in further enhancement in the section's strengths. The buckling load was increased by 39% when compared with the standard section, while the ultimate moment capacity was increased by 11% and when the cold working effect was included, the increase was a further 6%. When the section was optimised, the maximum increase of the buckling load was 111% (Candidate 5) while the maximum ultimate moment capacity was 17% (Candidate 6). The influence of the cold working was significant for all Candidates 4–6 with a maximum increase of 7%.

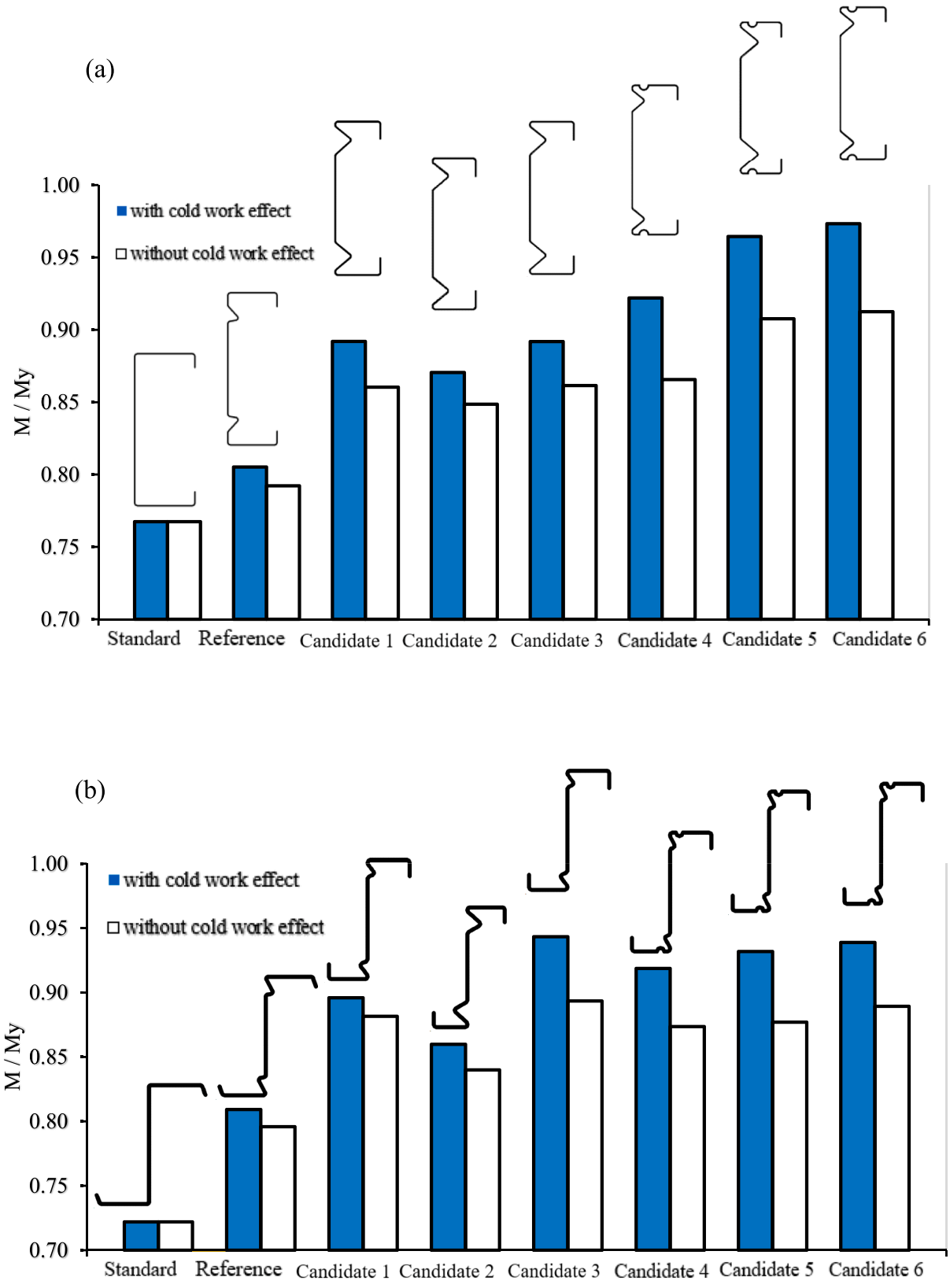

Fig. 13. Ultimate strength to yield ratio with the cold working effects and without the cold working effects for (a) channel cross sections with the depth of 170 mm, and (b) zed cross sections with the depth of 170 mm.

Table 9
The increase of flexural strengths of the reference and optimised sections in comparison to the standard sections including sections with flange stiffeners. The "Optimised" value presented is the maximum value from Candidates 1–3 for Reference (b) section, and Candidates 4–6 for Reference (c) section.

Section				Increase in flexural strength (%) In comparison to the standard section		
Depth	Flange stiffeners	Cross section	Type	Buckling load	Ultimate moment capacity	
				(kN)	M_u (kNm)	M_{uc} (kNm)
145 mm	Not included	Channel	Reference	33	15	16
			Optimised	65	27	29
		Zed	Reference	46	21	22
			Optimised	50	26	30
	Included	**Channel**	**Reference**	**55**	**33**	**38**
			Optimised	**118**	**43**	**50**
		Zed	**Reference**	**59**	**32**	**35**
			Optimised	**96**	**39**	**41**
170 mm	Not included	Channel	Reference	15	3	4
			Optimised	97	7	11
		Zed	Reference	21	4	6
			Optimised	110	14	20
	Included	**Channel**	**Reference**	**31**	**5**	**11**
			Optimised	**101**	**16**	**23**
		Zed	**Reference**	**39**	**8**	**14**
			Optimised	**111**	**14**	**20**

- Candidate 6 is the optimal solution, for both the channel and zed sections with the section depth of 170 mm gained most increase in the buckling and ultimate moment capacities without the cold working effect, and with the cold working effect. They were 84%, 13% and 20% for the channel section, respectively, and 110%, 17% and 23% for the zed section, respectively. It is noted that the stiffeners size was accounting for in the total developed length of the section and that, therefore, the flange width of the design candidate 6 is less than that of the reference section.

The following observations were made for both channel and zed sections with the depths of 145 mm and 170 mm:

- The cold working had modest effect in material strength in the flat regions of cold roll formed steel sections by on average 2.5%, but significantly enhanced material strength in the corner and stiffener bend regions by on average 18%.
- The extent of improved distortional buckling and ultimate strength benefit obtained from geometry and the cold working effects were dependent upon on the shapes and dimensions of the cross sections, the positions, shapes and dimensions of the stiffeners, and the amount of cold working area of the section corners and stiffener bends.
- The buckling load of the section was profoundly influenced by the shapes and dimensions of the cross section and the stiffeners. The optimised sections with two longitudinal web stiffeners in the web resulted in maximum enhancement in the buckling load of the channel and zed sections. The increase in the buckling load was significant for both the section depth of 145 mm (50–65%) and for the section depth of 170 mm (101%–120%). Adding one longitudinal stiffener to the top and bottom flanges of the section further increased the buckling load, with a greater increase for the section depth of 145 mm (75–131%) than for the section depth of 170 mm (97–111%).
- The ultimate strength of the section was significantly affected by the shapes, dimensions and material properties of the cross section and the stiffeners. The optimised sections with two longitudinal web stiffeners in the web provided noticeably enhancement in the moment capacity of the channel and zed sections. The increase in the moment capacity was significant for the section depth of 145 mm (23–32%), but less significant for the section depth of 170 mm (7–17%). The maximum cold working effect was 5–9% for the section depth of 145 mm, and 4–5% for the section depth of 170 mm. Adding one longitudinal stiffener to the top and bottom flanges of the section further increased the moment capacity, with a greater increase for the section depth of 145 mm (36–50%) than for the section depth of 170 mm (13–17%). In this case, the maximum cold working effect was 3–5% for the section depth of 145 mm, and 7% for the section depth of 170 mm.
- It revealed that, as illustrated in Table 9, for the section depth of 145 mm, the optimal designs provided up to 43% and 39% increase in flexural strength for the channel and zed sections, respectively; however, when the true material properties at the section corner and the stiffener's bend regions was included, the increase in flexural strength increased up to 50% and 41%, respectively. For the section depth of 170 mm, the optimal designs provided up to 16% and 14% increase in flexural strength for the channel and zed sections, respectively; however, when the true material properties at the section corner and the stiffener's bend regions was included, the increase in flexural strength increased up to 23% and 20%, respectively.

6. Conclusions

In this paper, the influence of cold working effects on mechanical properties and flexural strength of the cold roll formed sections were studied by experimental testing and combined Finite Element modelling and optimisation. A test program consisted of tensile tests and four-point bending tests were conducted to study the cold working effect in the section and stiffener's corners of cold roll formed sections and in the design optimisation. A practical method combining FE analysis and optimisation technique using DOE and response surface was adopted to obtain optimal designs for cold roll formed steel sections in flexural strength considering distortional buckling failure. In particular, the FE model was developed for replicating the section's flexural behaviour under four-point beam bending tests. The model included initial imperfections, geometry and the true material properties at the section and stiffener's corners and was then utilised to optimise the buckling and flexural strength of channel and zed sections with different section depths. Optimal cross-sectional shapes of the longitudinally stiffened channel and zed sections including flange stiffeners was finally achieved. The following conclusions were drawn based on the results of this study:

1) The results revealed the efficiency of the adopted optimisation approach to increase the ultimate strength of cold roll formed sections. The ultimate moment capacities of the optimised sections were significantly higher than those obtained from their standard and reference counterparts for the same amount of material used. This improvement was more evident for the zed sections which were less prone to distortional buckling failure mode.
2) The cold working effect in the corner and stiffener areas was insignificant on ultimate strength in the standard sections and only had a relevant influence at reference sections ultimate strength. The main reason for the low contribution of the cold working effects can be the higher distortional buckling slenderness and the relatively small area of the rounded corners compared to the total cross section area in the sections. On the other hand, the cold working effect significantly increased the ultimate strength of the optimised sections up to 7% and 9% for the channel and zed sections, respectively. In the optimised sections, several parts of the cross-section presented an equivalent strain higher than the yield strain, so the increase of the

yield strength in corner areas produced an increase of the flexural strength of the beams.

3) When both geometry and the cold working effect were considered in the optimisation process, optimal sections could be achieved with significant improvement in distortional buckling and ultimate strength. They were up to 118% and 53%, respectively, for the optimised channel section in comparison to the standard channel, and up to 96% and 38%, respectively, for the optimised zed section when compared to the standard zed section using the same amount of material.
4) When longitudinal stiffeners were included in the section flanges, the flexural strengths were profoundly enhanced. The buckling load was increased up to 131% when compared with the standard section, while the ultimate moment capacity was increased by 50% and the cold working effect of 5% for channel sections. The buckling load was increased up to 111% when compared with the standard section, while the ultimate moment capacity was increased by 36% and the cold working effect of 7% for zed sections. In addition, adding flange stiffeners to the sections with longitudinal web stiffeners generally increased further the section strength because this configuration led to a decrease in the distortional buckling slenderness of the sections. The reduction in distortional buckling slenderness generally has a positive impact, resulting in an increase in the ultimate load capacity of the sections. However, the levels of increase were largely dependent on the section depths and material properties through the increase could be small, as detailed in our previous studies [12,44].
5) The optimal cross-sectional shape recommended to have two longitudinal stiffeners at the web placed as much close as possible to the web-flange junctions, one longitudinal flange stiffeners placed near the web flange junctions as much as possible, and the relative dimensions of the sections as obtained from the optimisation process. The proposed shape could gain significant benefit from the geometry and the cold working effects.

CRediT authorship contribution statement

S.J. Qadir: Conceptualization, Methodology, Software, Validation, Formal analysis, Investigation, Writing - original draft, Data curation, Writing - review & editing, Visualization, Project administration. **V.B. Nguyen:** Conceptualization, Data curation, Formal analysis, Funding acquisition, Investigation, Methodology, Project administration, Resources, Software, Supervision, Validation, Visualization, Writing – original draft, Writing – review & editing. **I. Hajirasouliha:** Resources, Supervision, Funding acquisition, Conceptualization, Investigation, Validation, Writing - review & editing.

Declaration of Competing Interest

The authors declare that they have no known competing financial interests or personal relationships that could have appeared to influence the work reported in this paper.

Data availability

Data will be made available on request.

Acknowledgments

The authors would like to thank the Heavy Structures Laboratory, Department of Civil and Structural Engineering at The University of Sheffield for providing facilities and technical supports on conducting the experiments. The authors would also like to thank Hadley Industries plc. For providing investigation ideas, materials, technical advice and resources for the industrial cold roll formed sections.

References

[1] E. CEN, 1–3 Eurocode 3: Design of Steel Structures-Part 1–3: General Rules-Supplementary Rules for Cold-formed Members and Sheeting, European Committee for Standardization, 2006. Brussels.
[2] AISI S100–16, North American Specification for the Design of Cold-formed Steel Structural Members, 2016. Washington, DC.
[3] AS/NZS 4600, 2005 Cold-Formed Steel Structures, Standards Australia/Standards New Zealand, 2005.
[4] V.B. Nguyen, et al., Design of new cold rolled purlins by experimental testing and direct strength method, Thin-Walled Struct. 118 (2017) 105–112.
[5] H. Adeli, A. Karim, Neural network model for optimization of cold-formed steel beams, J. Struct. Eng. 123 (11) (1997) 1535–1543.
[6] J. Lee, et al., Optimum design of cold-formed steel channel beams using micro genetic algorithm, Eng. Struct. 27 (1) (2005) 17–24.
[7] J. Ye, et al., Optimum design of cold-formed steel beams using particle swarm optimisation method, J. Constr. Steel Res. 122 (2016) 80–93.
[8] J. Ye, et al., Development of more efficient cold-formed steel channel sections in bending, Thin-Walled Struct. 101 (2016) 1–13.
[9] M.R. Haidarali, D.A. Nethercot, Local and distortional buckling of cold-formed steel beams with both edge and intermediate stiffeners in their compression flanges, Thin-Walled Struct. 54 (2012) 106–112.
[10] S. Qadir, et al., Optimization of Flexural Strength for Cold Roll Formed Sections Using Design of Experiments and Response Surface Methodology, 2020.
[11] B. Schafer, T. Peköz, The behavior and design of longitudinally stiffened thin-walled compression elements, Thin-Walled Struct. 27 (1) (1997) 65–78.
[12] S. Qadir, et al., Optimal design of cold roll formed steel channel sections under bending considering both geometry and cold work effects, Thin-Walled Struct. 157 (2020), 107020.
[13] S. Qadir, et al., Shape optimisation of cold roll formed sections considering effects of cold working, Thin-Walled Struct. 170 (2022), 108576.
[14] M. Ashraf, L. Gardner, D. Nethercot, Strength enhancement of the corner regions of stainless steel cross-sections, J. Constr. Steel Res. 61 (1) (2005) 37–52.
[15] R.B. Cruise, L. Gardner, Strength enhancements induced during cold forming of stainless steel sections, J. Constr. Steel Res. 64 (11) (2008) 1310–1316.
[16] L. Gardner, D. Nethercot, Experiments on stainless steel hollow sections—Part 1: material and cross-sectional behaviour, J. Constr. Steel Res. 60 (9) (2004) 1291–1318.
[17] B. Rossi, S. Afshan, L. Gardner, Strength enhancements in cold-formed structural sections—part II: predictive models, J. Constr. Steel Res. 83 (2013) 189–196.
[18] B. Rossi, Mechanical Properties, Residual Stresses and Structural Behavior of Thin-Walled Stainless Steel Profiles, Université de Liège, 2008.
[19] P. van der Merwe, J. Coetsee, G. van den Berg, The Effect of Workhardening and Residual Stresses Due to Cold Work of Forming on the Strength of Cold-Formed Stainless Steel Lipped Channel Sections, 1990.
[20] P. Van der Merwe, G. van den Berg, Prediction of corner mechanical properties for stainless steels due to cold forming, in: CCFSS Proceedings of International Specialty Conference on Cold-Formed Steel Structures, 1992.
[21] M. Jandera, L. Gardner, J. Machacek, Residual stresses in cold-rolled stainless steel hollow sections, J. Constr. Steel Res. 64 (11) (2008) 1255–1263.
[22] M. Jandera, J. Machacek, Residual stress influence on material properties and column behaviour of stainless steel SHS, Thin-Walled Struct. 83 (2014) 12–18.
[23] S. Afshan, B. Rossi, L. Gardner, Strength enhancements in cold-formed structural sections—part I: material testing, J. Constr. Steel Res. 83 (2013) 177–188.
[24] L. Gardner, D.A. Nethercot, Experiments on stainless steel hollow sections—part 1: material and cross-sectional behaviour, J. Constr. Steel Res. 60 (9) (2004) 1291–1318.
[25] K.W. Karren, Corner properties of cold-formed steel shapes, J. Struct. Div. 93 (1) (1967) 401–432.
[26] N. Abdel-Rahman, K. Sivakumaran, Material properties models for analysis of cold-formed steel members, J. Struct. Eng. 123 (9) (1997) 1135–1143.
[27] L. Gardner, N. Saari, F. Wang, Comparative experimental study of hot-rolled and cold-formed rectangular hollow sections, Thin-Walled Struct. 48 (7) (2010) 495–507.
[28] J. Bonada, et al., Influence of the cold work effects in perforated rack columns under pure compression load, Eng. Struct. 97 (2015) 130–139.
[29] W. Quach, J. Teng, K.F. Chung, Effect of the manufacturing process on the behaviour of press-braked thin-walled steel columns, Eng. Struct. 32 (11) (2010) 3501–3515.
[30] V.B. Nguyen, et al., Compression tests of cold-formed plain and dimpled steel columns, J. Constr. Steel Res. 69 (1) (2012) 20–29.
[31] V.B. Nguyen, et al., Finite element simulation on mechanical and structural properties of cold-formed dimpled steel, Thin-Walled Struct. 64 (2013) 13–22.
[32] V.B. Nguyen, et al., Analysis and design of cold-formed dimpled steel columns using finite element techniques, Finite Elem. Anal. Des. 108 (2016) 22–31.
[33] F. Wang, Numerical Studies of Residual Stress in Cold Formed Steel Sigma Sections, University of Birmingham, 2015.
[34] Y.B. Kwon, G.J. Hancock, Tests of cold-formed channels with local and distortional buckling, J. Struct. Eng. 118 (7) (1992) 1786–1803.
[35] J. Ye, S.M. Mojtabaei, I. Hajirasouliha, Local-flexural interactive buckling of standard and optimised cold-formed steel columns, J. Constr. Steel Res. 144 (2018) 106–118.
[36] K.W. Karren, Corner properties of cold-formed shapes, J. Struct. Div. 93 (1) (1967) 401–433.
[37] W. Quach, J. Teng, K. Chung, Effect of the manufacturing process on the behaviour of press-braked thin-walled steel columns, Eng. Struct. 32 (11) (2010) 3501–3515.

[38] V.B. Nguyen, et al., Analysis and design of cold-formed dimpled steel columns using finite element techniques, Finite Elem. Anal. Des. 108 (2016) 22–31.
[39] J. Lee, S.-M. Kim, H.S. Park, Optimum design of cold-formed steel columns by using micro genetic algorithms, Thin-Walled Struct. 44 (9) (2006) 952–960.
[40] Y. Shifferaw, B. Schafer, Inelastic bending capacity of cold-formed steel members, J. Struct. Eng. 138 (4) (2012) 468–480.
[41] B.W. Schafer, T. Peköz, Computational modeling of cold-formed steel: characterizing geometric imperfections and residual stresses, J. Constr. Steel Res. 47 (3) (1998) 193–210.
[42] B.W. Schafer, Z. Li, C.D. Moen, Computational modeling of cold-formed steel, Thin-Walled Struct. 48 (10−11) (2010) 752–762.
[43] B. Durakovic, Design of experiments application, concepts, examples: state of the art, Periodic. Eng. Nat. Sci. 5 (3) (2017).
[44] V.B. Nguyen, M.A. English, The optimisation of thin-walled cold rolled products using finite element modelling and design of experiment, in: The 8th International Conference on Thin-Walled Structures ICTWS2018, Lisbon, Portugal, 24-27 July 2018, 2018.